HHS Public Access

Author manuscript

ACS Nano. Author manuscript; available in PMC 2023 November 22.

Published in final edited form as:

ACS Nano. 2022 November 22; 16(11): 17708–17728. doi:10.1021/acsnano.2c08164.

Natural Piezoelectric Biomaterials: A Biocompatible and Sustainable Building Block for Biomedical Devices

Ruoxing Wang,

Department of Materials Science and Engineering, University of Wisconsin-Madison, Madison, Wisconsin 53706, United States

Jiajie Sui,

Department of Materials Science and Engineering, University of Wisconsin-Madison, Madison, Wisconsin 53706, United States

Xudong Wang

Department of Materials Science and Engineering, University of Wisconsin-Madison, Madison, Wisconsin 53706, United States

Abstract

The piezoelectric effect has been widely observed in biological systems, and its applications in biomedical field are emerging. Recent advances of wearable and implantable biomedical devices bring promise as well as requirements for the piezoelectric materials building blocks. Owing to their biocompatibility, biosafety, and environmental sustainability, natural piezoelectric biomaterials are known as a promising candidate in this emerging field, with a potential to replace conventional piezoelectric ceramics and synthetic polymers. Herein, we provide a thorough review of recent progresses of research on five major types of piezoelectric biomaterials including amino acids, peptides, proteins, viruses, and polysaccharides. Our discussion focuses on their structure- and phase-related piezoelectric properties and fabrication strategies to achieve desired piezoelectric phases. We compare and analyze their piezoelectric performance and further introduce and comment on the approaches to improve their piezoelectric property. Representative biomedical applications of this group of functional biomaterials including energy harvesting, sensing, and tissue engineering are also discussed. We envision that molecular-level understanding of the piezoelectric effect, piezoelectric response improvement, and large-scale manufacturing

Corresponding Author: **Xudong Wang –** Department of Materials Science and Engineering, University of Wisconsin-Madison, Madison, Wisconsin 53706, United States; xudong.wang@wisc.edu.

Complete contact information is available at: https://pubs.acs.org/10.1021/acsnano.2c08164

The authors declare no competing financial interest.

VOCABULARY

Piezoelectric effect, a material's property that electrical polarization is generated in response to strains; piezoelectric coefficient, the parameter of a piezoelectric material that quantifies the polarization generated under applied mechanical stress or the mechanical strain experienced under an electrical field. The larger the piezoelectric coefficient, the higher the energy conversion efficiency; piezoresponse force microscopy, a functional atomic force microscopy mode, probing electromechanical properties of materials in addition to the sample topography; natural biomaterials, materials naturally exist in biological systems, which typically carry certain functions; nanogenerator, a device that converts mechanical energy into electricity using nanomaterials or from the nanoscale

are three main challenges as well as research and development opportunities in this promising interdisciplinary field.

Graphical Abstract

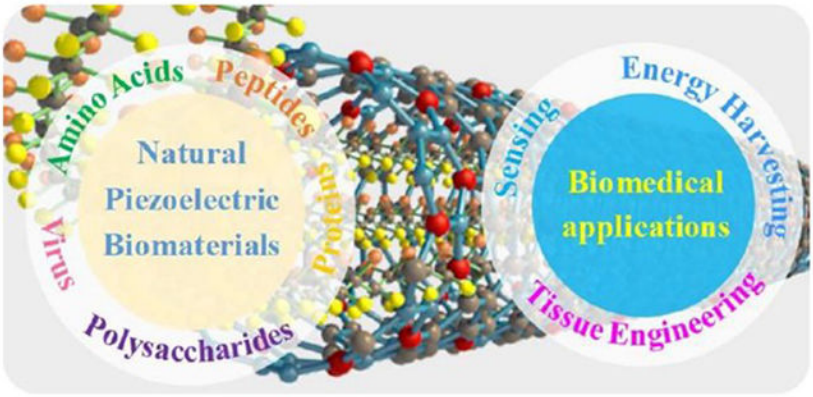

Keywords

piezoelectric; natural biomaterials; sustainable materials; biomedical devices; nanogenerator; flexibility; amino acids; proteins; polysaccharides

1. INTRODUCTION

The piezoelectric effect is a phenomenon that certain materials can generate electrical polarization in response to strains. It was discovered by the Curie brothers in 1880 using quartz and Rochelle salt crystals.[1] The origin of this phenomenon was found to be the lack of inversion symmetry in crystalline structures,[2] which further inspired the discoveries of piezoelectric properties in other materials with noncentral symmetric lattices, such as perovskites and wurtzite.[3–5] These inorganic piezoelectric materials have been exploited in many practical applications, including igniters,[6] sensors,[7] actuators,[8] and energy harvesters.[9,10] Piezoelectricity can also be generated in some crystalline organic (particularly polymer) materials, represented by polyvinylidene fluoride (PVDF). The piezoelectric effect in polymers is induced by the alignment of molecular dipoles in the polymer chains.[11,12] The piezoelectric polymers have a much lower Young's modulus compared to ceramics, offering a flexible building block for piezoelectric devices, which broadens their potential applications toward the area of biomedical devices.[13] Nowadays, researchers are continuously challenged to advance the properties of piezoelectric materials through material design and engineering to meet various requirements from the complex biological world.

Indeed, the piezoelectric effect has been observed from diverse biological systems. Since polarization was discovered in wool and hair in 1941,[14] piezoelectricity has been discovered in wood,[15] bone,[16,17] tendon,[18] skin,[19] and many other asymmetric biological components.[20–22] More importantly, the bioelectricity generated from the piezoelectric effect exerts physiological significance in living systems.[22–25] For example, the human tibia

generates a 300 μV piezoelectric potential from walking.[26,27] The endogenous electric field of living bone influences its remodeling and growth.[28] According to Wolff's law, bone can adeptly reconstruct in response to subjective stress via deposit and reinforce at areas of immense stress.[29,30] Besides, piezoelectric charges in the lung generated during respiration could help bind oxygen to hemoglobin.[31] The mechanically activated ion channels on the membrane, the corresponding proteins named PIEZO1 and PIEZO2, were identified as the major mechanical transducer in somatic nerves and are vital for human perception of touch and proprioception.[32–34] The discovery of receptors for touch was awarded the Nobel Prize in physiology or medicine in 2021, illustrating the importance of the conversion between mechanical stimuli and electricity in living systems and further attracting much more attention in this field.

Therefore, piezoelectric materials that mimic the natural process of biological systems are envisioned as promising approaches for biomedical applications such as tissue repair and regeneration.[27] The medically implantable and wearable devices in biological systems are an emerging research direction for piezoelectric materials. To be applied in biological systems and interface with soft biological tissues, the materials must be flexible, biocompatible, and even biodegradable.[35–37] However, most conventional piezoelectric materials are challenging due to their poor biosafety and biocompatibility. Inorganic piezoelectric materials are intrinsically rigid and may contain hazardous elements, while synthetic piezoelectric polymers are nonbiodegradable and may cause the release of toxic molecules such as hydrogen fluoride during its synthesis and decomposition processes.[38–41] Hence, natural piezoelectric biomaterials, i.e., materials originated from the biological system itself, have recently attracted considerable interests for biomedical applications because they are naturally flexible, biocompatible, and mostly biodegradable. The reported natural piezoelectric biomaterials mainly include small biomolecules such as amino acids[42] and peptides,[43] polymers such as proteins[44,45] and polysaccharides,[46,47] and viruses,[48] as summarized in Figure 1 (to simplify the discussion, they are called piezoelectric biomaterials in the rest of this review). Their piezoelectric crystalline phases have been successfully synthesized and demonstrated intriguing application potential for biomedical energy harvesting,[43] sensing,[49] and tissue engineering.[50,51] Nevertheless, the piezoelectric response of biomaterials is relatively weak compared to piezoelectric ceramics and even polymers.[52] Besides, the large-scale assembly and domain alignment of piezoelectric biomaterials remain challenging.[37] To date, several strategies have been demonstrated to boost their performances by molecular design, fabrication of heterostructure, and adjustment of orientation and polarization direction.[2,53] With the continuous efforts on enhancement of properties and scalable production, piezoelectric biomaterials are expected to make significant advancements in biomedical engineering.

Herein, we provide a thorough review of recent progress in the preparation and properties of piezoelectric biomaterials and their applications in biomedical fields. We overview the piezoelectric properties from these five major types of biomaterials including amino acids, peptides, proteins, viruses, and polysaccharides. The strategies to improve their piezoelectric performances will be discussed. Subsequently, their representative biomedical applications will be discussed, including energy harvesting, sensing, and tissue engineering. Toward the end, we will provide our perspectives and discuss the challenges and opportunities for

the future exploration of piezoelectric biomaterials in biomedical applications. This review intends to provide a helpful and forward-looking reference and facilitate the development of emerging piezoelectric biomaterials.

2. AMINO ACIDS AND PEPTIDES

We start our discussion of piezoelectric biomaterials with amino acids, the fundamental building blocks of proteins, which further serve as an essential component of life. The general molecular structure of amino acids contains an amino group ($-NH_2$) and a carboxyl group (−COOH), along with a side chain (R) specific to each amino acid (Figure 2a). There are 20 types of amino acids occurring in natural proteins. Among them, 17 amino acids and their compounds have been confirmed to be piezoelectric experimentally, except for glutamine, phenylalanine, and tryptophan.[54,55] Piezoelectricity in amino acid crystals is a result of the accumulation of dipole moments pointing from carboxyl group to amino group under influence of mechanical stress. A noncentrosymmetric crystal structure of most amino acids allows a net polarization to develop without canceling each other, which generates piezoelectricity in bulk scale. As piezoelectricity is a thirdrank property tensor, crystal symmetry affects the values of piezoelectric coefficients in longitudinal, transverse, and shear directions. The number of nonzero coefficients in each direction vary among amino acids that belong to different crystal classes.

In 1970, Vasilescu et al. performed piezoelectricity test on the common 20 types of amino acids, all of them can exhibit piezoelectricity in a specific phase.[54] Amino acids could exhibit a wide range piezoelectricity from 0.5 pC/N to 178 pC/N based on theoretical and experimental studies.[3,4] However, the strong piezoelectricity was only predicted or measured in shear directions, which is less suitable for practical applications. The highest longitudinal charge coefficient d_{33} is predicted in γ-glycine crystal of 10.4 pC/N, in the same level of quartz crystals and zinc oxide. Here, we will primarily focus on glycine to discuss the piezoelectric property and structure relationships.

Glycine is the simplest and the only nonchiral amino acid, where R is an H atom. Glycine has three types of crystal structures, namely α, β, and γ (Figure 2b).[56] The glycine molecules in α-glycine crystals arrange in centrosymmetric configuration of space group $P2_1/c$, and so the α-glycine crystals are not piezoelectric materials, while it may exist surface piezoelectricity by water incorporation.[57,58] The β-glycine and γ-glycine have been found to be piezoelectric, which belong to the noncentrosymmetric space groups $P2_1$ and $P3_2$, respectively.[59,60] The β-glycine was predicted to have a significantly high shear piezoelectric coefficient (d_{16}) of 195 pm V^{-1}, which was confirmed experimentally through resonance piezoelectric measurements by using an impedance analyzer.[42] The obtained d_{16} value of β-glycine was 178 ± 11 pm V^{-1} as labeled in Figure 2c, which is comparable to conventional piezoelectric ceramics, such as $BaTiO_3$[66] and soft-PZT cermaics,[67] and several times higher than maximum piezoelectric coefficients of biological piezoelectric materials like collagen,[61] γ-glycine,[62] PVDF polymers,[63,64] and peptide nanotubes. Such a high shear piezoelectricity could be attributed to the supramolecular packing that contributes to the shear elastic response with a high shear compliance, leading to electric dipoles acting along a particular direction.[24,30] Nevertheless, aside from the limited practical situations for using

the shear effect, the wide application of β-glycine is also limited by its thermodynamic instability, as the metastable polymorph can spontaneously transform into stable α- or γ-phases under ambient conditions.[68,69] To stabilize the β-phase and improve the flexibility, compositing the glycine crystals with elastomeric dielectric polymers was a typical strategy. In 2020, Hosseini et al. fabricated homogeneous and extremely stable β-glycine crystals in a chitosan matrix by a simple solvent-casting method.[49] As shown in Figure 2e, the spherulite of β-glycine could exhibit in noncrystalline regions of chitosan. The β-glycine crystals were stabilized within the chitosan media due to the alteration of crystallization kinetics. The as-prepared β-glycine/chitosan film was applied as a biocompatible and flexible piezoelectric pressure sensor.

Because most available mechanical energy sources exist as compressive or tensile forces, the longitudinal piezoelectric tensors are considered more significant and normally more practical.[25] The longitudinal piezoelectric coefficient d_{22} in β-glycine was predicted to be -5.7 pm V^{-1} and was measured as -4.7 pm V^{-1} by using a piezometer.[42] Isakov et al. reported the electrospinning of β-glycine/poly(vinyl alcohol) (PVA) nanofibers that formed highly oriented and stable β-glycine nanocrystals within the polymer fibers.[70] The effective piezoelectric coefficient was measured by piezoresponse force microscopy (PFM) at 12.5 pm V^{-1}. However, the measured value could be a combination of both longitudinal and shear responses, due to the heterogeneous distribution of the local electric field caused by cylindrical geometry of fiber.

Different from β-glycine, γ-glycine allows three longitudinal nonzero piezoelectric coefficients, d_{11}, d_{22}, and d_{33}. The predicted value of d_{33} was 10.4 pm V^{-1}, which was 2-fold higher than the longitudinal piezoelectric coefficient in β-glycine and at the same level to the highest reported value of zinc oxide.[42,72] The measured values of d_{33} in γ-glycine, 9.93 pm V^{-1} by using a piezometer (Figure 3a) and 10 pm V^{-1} by a PFM, agreed well with the predicted value.[42,62] In addition to the piezoelectricity, Heredia et al. reported robust and continuous nanoscale ferroelectricity in γ-glycine.[62] As shown in Figure 3b, the well-defined piezoresponse hysteresis loop indicates the polarization switching of ferroelectric domains in γ-glycine under electrical field, indicating potential applications of γ-glycine in bioelectronic logic, sensors, and memory devices.[25,62] However, some following papers disputed that ferroelectricity in Heredia's work could actually not only from γ-glycine.[73] The integral characterization methods in Heredia's work, X-ray diffraction spectra and Fourier transform infrared (FTIR) spectroscopy, allow detection of tiny amount phases in a mixture. PFM has been performed to determine piezoelectricity of individual phases distinguished by spectral analysis of confocal Raman microscopy (CRM).[74] In addition, in Heredia's work, the molecular-dynamic simulations were performed suggesting the switching of glycine molecules occur between 4 V nm^{-1} and 8 V nm^{-1}, while the experimental data shown the switching occurred at an electrical field of 1 V nm^{-1}.[62]. Although computing models predicted the coercive field of β-glycine is about 1 V nm^{-1},[75,76] another recent study obtained similar results of 1 V nm^{-1} for γ-glycine.[77] The ferroelectricity of glycine requires further investigations to clearly identify the phases and carefully test the ferroelectric properties. However, β-glycine is unstable, limiting its experimental studies and applications. Besides, it is not easy to obtain γ-glycine from a neutral aqueous solution due to the inhabitation from α-glycine crystallization.[12] An

acidic or basic solution is typically required to grow single crystals of γ-glycine.[13,14] For neutral solutions, γ-glycine could also be obtained with inhibitor additives, [13,15] adding external laser light[16] or electric field[17] or by slow evaporation from microdroplets.[12] Nevertheless, aiming at flexible piezoelectric device applications, it is still challenging to achieve large-scale aligned crystalline domains in flexible films that can offer appreciable bulk piezoelectricity.

Recently, Yang et al. developed a self-assembly strategy for synthesis of flexible heterostructured PVA-glycine-PVA thin films in wafter scale (Figure 3c).[37] The synthesis was based on a mixed aqueous solution of both PVA and glycine. Due to the solubility difference, PVA films were precipitated out preferentially as a result of the salting out effect. The hydrogen bonding between the carboxyl group of PVA and hydroxyl group of glycine then led to the directional nucleation and growth of γ-glycine crystals across the entire film (Figure 3d). The as-received glycine-PVA films exhibited macroscopic piezoelectricity with a measured d_{33} of 5.3 pm V^{-1} and improved flexibility, offering a simple and promising solution for preparing high-performance piezoelectric biomaterials for flexible devices.

The d_{33} demonstrated in Yang's work reached more than 50% of the theoretical value, while still left a big room for improvement. One of the main reasons for their materials not showing higher d_{33} is that the piezoelectric polar [001] direction was not aligned perpendicularly to the film surface. Because the misalignment was due to the tilted interface where the nucleation occurs, Sui et al. presented a modified strategy to move the nucleation site of γ-glycine crystals to the flat interface area.[71] In their approach, a hydrophilic wall was added around the liquid precursor film. This changed liquid film edge from a convex surface to a concave surface. The negative surface curvature became less favorable for nucleation compared to a flat surface due to decreased water evaporation rate (Figure 3e). Consequently, nucleation started to form at the center flat area, with the (001) facets facing the interface and thereby aligned the piezoelectric polarization preferably. Therefore, the as-prepared γ-glycine films exhibited an improved d_{33} of 6.13 pC/N, the highest bulk value that has even been reported.

Peptides are short chains of amino acids, so that they share many structural and property features of amino acids. Thereby, organized peptide molecules also exhibit structure-dependent piezoelectric properties,[25,81] such as diphenylalanine (FF),[65] fluorenylmethyloxycarbonyl diphenylalanine (Fmoc-FF),[82] cyclo-glycine-tryptophan (cyclo-GW),[83] cyclo-phenylalanine-tryptophan (cyclo-FW),[84] and bis-cyclic-β-peptide.[85] Similar to amino acids, the piezoelectricity is also originated from the internal electrical dipoles in between the amino and carboxyl groups. The relatively large molecules and more functional groups in peptides can introduce more complex intermolecular interactions than amino acids and thus lead to different self-assembly phenomena in molecule ordering and piezoelectric performance.[83,86]

Among these peptides, FF is one of the most studied piezoelectric peptide because of its simple structure, notable stiffness, and high piezoelectricity.[87] It consists two naturally occurring amino acid phenylalanine (Phe) with a structure of NH_2-Phe-Phe-COOH. The FF crystal has no inversion symmetry center with the space group $P6_1$ that enables

its piezoelectricity.[65] The FF dipeptide can frequently self-assemble into nanowires and nanotubes structures driven by intermolecular hydrogen bonding, electrostatic force, solvent-mediated force, and π–π stacking.[79,88,89] Kholkin et al. synthesized FF nanotubes that were assembled in pairs with oppositely directed polarizations (Figure 4a).[65] PFM measurements detected the in-plane signal along the tube axis, and uncovered its shear component of the piezoelectric coefficient (d_{15}) from nanotube B. After lateral signal calibration, the effective d_{15} for a 100 nm FF nanotube was determined to be ~35 pm V^{-1}, about half of bulk $LiNbO_3$, a common lead-free piezoelectric ceramic (Figure 4b). Strong piezoelectric anisotropy of piezoelectric coefficients was measured from FF microtubes by PFM with d_{15} of 80 ± 15 pm V^{-1} and d_{33} of 18 ± 5 pm V^{-1}.[90]

Moving from nanoscale characterization to macroscopic applications, researchers devoted efforts to the large-scale fabrication of aligned and unipolarized FF films.[43,78,91] Nguyen et al. successfully controlled the polarization of FF peptide microrods during self-assembly process under an external applied electric field.[43] The obtained FF microrods had preferred polarization along the applied field without significant morphology changes (Figure 4c–e). The aligned vertical microrods arrays exhibited improved piezoelectricity with d_{33} = 17.9 pm V^{-1}. Lee et al. developed a facile meniscus-driven self-assembly strategy fabricate large-scale aligned FF nanotube arrays.[78] As shown in Figure 4f, a substrate was pulled vertically from a FF solution. During the process, rapid evaporation at the air–liquid–solid interface leads to a locally concentration gradient of FF molecules and subsequent nanostructure formation along the pulling direction. A strong shear piezoelectric coefficient d_{15} related to the in-plane signal was measured from the horizontally aligned FF nanotubes to be 46.6 pm V^{-1} by PFM. The similar mechanism was also applied in three-dimensional (3D) printing of FF peptide with free patterns.[79] During the 3D printing process, rapid solvent evaporation enabled continuous solidification of FF under a designed path guided by femtoliter ink meniscus formed on a glass micropipette, and the subsequent crystallization occurred by heat treatment. This strategy enabled the creation of various 3D architectures of crystalline FF crystals (Figure 4g,h). The as-printed FF structures exhibited a notable out-of-plane piezoresponse after annealing as revealed by PFM measurements (Figure 4h). The effective out-of-plane piezoelectric coefficient d_{eff} of the annealed FF line was estimated to be 7.23 ± 0.23 pm V^{-1}.

In addition, the FF peptides can be fabricated via several other approaches, including microfluidic, capillary, and inkjet printing.[92–95] Recently, the preparation of layered FF was achieved by Zelenovskii et al. via a coassembly of L,L- and D,D-enantiomers of FF (LFF and DFF) monomers.[80] The crystal structure of LDFF is formed by stacking layers of LFF and DFF in alternating sequence (Figure 4i). The bilayered LDFF structure exhibited a strong piezoelectric response with the d_{33} = 20 pm V^{-1} (Figure 4k) and enhanced stability than conventional FF nanomaterials. The peptide coassembly has been applied to enhance piezoelectricity.[96] Yuan et al. reported that compared with pure FF peptides, the coassembled peptides of FF and phenylalaninetryptophan showed a significant 38% increase in piezoelectric coefficient. Based on the structure of FF, Basavalingappa et al. designed highly aromatic dipeptides consisting of additional phenyl rings by substituting one phenylalanine amino acid in the FF with the β,β-diphenyl-Ala-OH (Dip) residue.[87] Among the studied aromatic-rich dipeptides, *tert*-butyloxycarbonyl (Boc)-Dip-Dip exhibits excellent

piezoelectric performance including a significant molecular dipole inside a relatively small unit cell with a significant effective piezoelectric coefficient $d_{33,eff}$ = 73.1 ± 13.1 pm V^{-1}. This impressive value shows the promise of introducing large molecular groups, such as phenyl rings, to enhance the piezoelectric responses, along with the similar concept, by adding fluorenyl-methoxycarbonyl (Fmoc) as side group to the chain of FF peptides as Fmoc-FF nanotubes with the d_{15} of 33.7 ± 0.7 pm V^{-1}.[82] Besides, density functional theory (DFT) calculation recently predicted that cyclo-GW peptides may demonstrate a high piezoelectric coefficient d_{16} of 13.8 pm V^{-1}.[83]

3. PROTEINS AND VIRUSES

Proteins are complex macromolecules that comprise of multiple amino acids. They play essential roles in the structure, function, and regulation of the body, where their activities are determined by the specific 3D structure and sequence of amino acids. Piezoelectricity has been observed in various proteins, such as collagen, silk, elastin, and lysozyme. Due to the high complexity of the chemistry and structure, the mechanism and strength of the piezoelectricity vary substantially from one to the other. Here, we will focus our discussion on collagen, silk, and elastin, which are commonly studied piezoelectric proteins showing representative relationships among their structure, morphology and piezoelectricity. Although the structures of viruses are much more complicated, the piezoelectricity of viruses primarily come from their protein components. Therefore, viruses are discussed together in this section as well.

Collagen is the most sufficient structural protein in animals, accounting for about one-third of the total protein components, which can be found in bone, tendon, skin, and muscle.[24,25,98] Collagen-based products have been widely approved by the U.S. Food and Drug Administration (FDA) for commercial and clinical use.[97] Collagen has a hierarchical microstructure. At the basic level, the polypeptide chains consist of three-amino acid repeating motif G-X-Y, where G is glycine and X and Y can be any amino acid but usually proline and hydroxyproline.[99,102] Spatially, collagen molecule has a triple helix structure formed by three twisted polypeptide chains, as shown in Figure 5a.[56,97] The interstrand hydrogen bonds helped protein form secondary structure and stabilize the triple helix (Figure 5b).[98,103] At a more detailed level, a collagen fibril is composed of collagen molecules quarterstagger arranged axially at a periodicity D of about 67 nm (Figure 5c). In reality, gap and overlap regions exist along the fiber axial direction from such arrangement, resulting in a 20% lower packing density in gap region than in overlap region.[100]

The piezoelectricity in collagen fibrils has been investigated since the piezoelectric effect of bones was discovered in 1957.[44,104–106] It is generally accepted that piezoelectricity in collagen is attributed to the accumulation of dipole moment along the peptide chain and hydrogen bonding from supramolecular packing.[24,100,107] Minary-Jolandan and Yu probed the electromechanical property of a single isolated type I collagen fibril by using PFM.[100] As shown in Figure 5d, the PFM images revealed the presence of shear piezoelectric responses in the collagen fibril. Moreover, a periodic modulation of the piezoresponse amplitude existed due to the bonding pattern of the overlap (brighter contrast) and gap (darker contrast) regions along axial direction. The linear relationship between the shear

piezoresponse and the applied voltage measured on the overlap region, shown in Figure 5e, revealed a linear relationship between piezoresponse and applied voltage of the overlap region and an effective piezoelectric constant of ~2 pm V^{-1}. Denning et al. compared the shear piezoelectric coefficients between type I and type II collagen fibrils.[101] The D-periodicity of collagen fibrils was visible in the 3D AFM topography images (Figure 5f). By calculating the slopes of PFM amplitude curves, the shear piezoelectric coefficient d_{15} of type II fibrils was determined to be ~28–32% lower than that measured for collagen type I. The highest piezoelectric coefficient measured in collagen was $d_{14} = -12$ pm V^{-1} from rat tail tendons at the nanoscale.[24,108]

Silk is another attractive piezoelectric biomaterial with outstanding biomedical compatibility, tunable biodegradability, and high flexibility.[109,112] Silkworm cocoons are made from two main proteins: fibroin and sericin.[110] Sericin is commonly removed during degumming process, and silk fibroin is mainly responsible for holding the fibrous fibroin.[110,113] Silk fibroin presents crystalline polymorphism (Figure 6a), where silk I predominantly has a α-helix structure with an orthorhombic unit cell; silk II has antiparallel β-sheet structure with a monoclinic unit cell; and unstable silk III exists with an overall trigonal unit cell in regenerated silk fibroin thin films at the air/water interface.[45,110,112,114] The inherent piezoelectricity of silk fiber bundles was reported by Fukada in 1956, and the observed piezoelectric response was ~1 pC N^{-1}.[115] This rather low piezoelectric property could be a result of the low crystallinity and mixed phases. Therefore, over decades, silk has been mostly considered and studied as a structural material rather than a piezoelectric material. In recent years, mostly driven by the flexible functional biomaterial research, more attention has been focused on its piezoelectric property. In 2011, Yucel et al. studied the structural origins of shear piezoelectricity in silk films based on the composition of β-sheet and uniaxial molecular orientation.[45] They demonstrated that the piezoelectricity of silk could be modulated by controlling the processing parameters and the aligned silk II film could achieve a shear piezoelectric constant d_{14} of 1.5 pC N^{-1} (Figure 6b). Sencadas et al. processed silk fibroin by electrospinning (Figure 6c).[110] This as-spun highly oriented and electrically poled crystalline structure yielded a substantially high piezoelectric constant d_{33} of 38 pm V^{-1}. With such a high performance, silk may enable an excellent flexible biomaterial film that offers both strong mechanical and piezoelectric properties.

Elastin is an extracellular matrix protein present in all connective tissues and is particularly abundant in tissues or organs under constant mechanical stress, such as lungs, skin, and blood vessel walls (Figure 6d).[116,117] Liu et al. confirmed the piezoelectricity in aortic elastin by PFM (Figure 6e) with the measured piezoelectric coefficient on the order of 1 pm V^{-1}.[111,117] Jiang et al. estimated the effective piezoelectric coefficient of murine lung in the order of 0.1 pm V^{-1}.[31] In addition to piezoelectricity, elastin is ferroelectric, while collagen appears to be nonswitchable, indicating the potential electrical poling to enhance elastin piezoelectric strength.[24,111,117] Elastin monomers are found to have intrinsic polarization at a similar level to classic perovskite unit cells.[111]

Lysozyme, different from the fibrous proteins, is a globular protein in egg whites and mammalian secretions. Stapleton et al. reported piezoelectricity, ferroelectricity, and pyroelectricity in lysozyme films.[118–120] The average piezoelectric coefficients of

monoclinic and tetragonal lysozyme films were 0.94 pm V^{-1} and 3.16 pm V^{-1}, respectively.[119]

A **virus** is an infectious microbe consisting of a segment of nucleic acid by a protein coat, the capsid. The lack of inversion symmetry in capsid protein structure endows the piezoelectricity of certain viruses. The M13 bacteriophage (phage) is an example of a virus that has piezoelectric properties. As shown in Figure 7a, the M13 phage has a long rod-like shape covered by thousands of a major coat protein (pVIII) and five minor coat proteins (pIII and pIX) at each end.[48] The piezoelectricity is mainly from pVIII in an α-helical structure with a dipole moment pointed from the amino- to the carboxyterminal. Lateral PFM images in Figure 7b,c show detected piezoelectricity of monolayer phage film in both axial and radial directions, revealing the contribution from radial component independent of orientation, respectively.

The pVIII N-terminus could be genetically engineered with glutamate (E) by recombinant DNA techniques. The engineered 4E-phage monolayer exhibited the out-of-plane piezoelectric response d_{eff} of 0.70 ± 0.05 pm V^{-1}. The d_{33} value of 4E-phage film with >100 nm thickness was estimated to be 7.8 pm V^{-1} which was much greater than the d_{33} = 1.1 pm V^{-1} of collagen films (Figure 7d). Compared with the laterally assembled phages, Shin et al. developed a template-assisted self-assembly method to fabricate M13 phage nanopillars with enhanced piezoelectric outputs in the axial direction.[121] Highly vertically self-assembled phage nanopillars bundles were obtained by extruding the suspension into a porous template at precisely controlled speeds (Figure 7e) and removing the template afterward (Figure 7f). The d_{33} value of engineered phage nanopillars was estimated to be 10.4 ± 0.5 pm V^{-1} from the relation for the quasi-static piezoelectric coefficient,[123] higher than phages films. Lee et al. developed another capillary force-driven template-assembly strategy to phage pillars over a larger area.[122] The phage solution was deposited on a nickelnitrilotriacetic acid (Ni-NTA) modified surface with a micropatterned polydimethylsiloxane (PDMS) template. The M13 phage engineered with hexa-histidine (6H) was able to bind strongly with the substrate, which induced an upward axial force to guide the self-assembly of phages (Figure 7g). The vertically aligned phages structure exhibited unidirectional polarization with an effective out-of-plane $d_{33,\text{eff}}$ of 13.2 pm V^{-1}, which was three times higher than film structures (Figure 7i). The assembly behaviors of M13 phage were further explored by several works, suggesting the potential for scalable and efficient fabrication of M13 phage in piezoelectric applications.[124,125]

From above discussion, we can see that the piezoelectricity from proteins is generally weak and dominated by the shear-based responses. This can be partially attributed to their large and complex molecules, which makes the long-range ordering of high density molecular dipoles rather challenging. For viruses, as represented by phage, their more rigid structure may help the alignment of polarization in their protein building blocks, and therefore higher piezoelectric responses have been detected. Nevertheless, understanding of the piezoelectricity in both materials is still fairly limited. Rather than these very basic structure and piezoresponse characterizations, no practical applications have been demonstrated so far.

4. POLYSACCHARIDES

Polysaccharides are the most abundant natural carbohydrates which are composed of monosaccharides with a general formula of $C_x(H_2O)_y$. They are widely found in food, plants, and animals, in the form of storage and structural polysaccharides. This group of materials are probably the most broadly studied piezoelectric biomaterials. There are also number of review articles focusing on the piezoelectric property of polysaccharides, particularly cellulose nanocrystals (CNC).[126–130] Therefore, here we do not intend to reiterate all the details of recent progresses of piezoelectric CNC-related materials. Instead, we focus on a few key aspects of polysaccharides' structure, alignment, and properties in comparison to other materials discussed above to bring up a full spectrum of piezoelectric biomaterials for readers to reference.

The research interests in piezoelectric polysaccharides stem from the intrinsic piezoelectricity of wood.[15,138] In 1955, Fukada studied the piezoelectric effect of wood and brought up that it could be attributed to the aligned uniaxial fibrous structure of cellulose crystallites and their monoclinic symmetry.[138] Since then, much effort has been devoted to assembling highly aligned cellulose films for piezoelectric applications. Figure 8a shows the schematic representation of nanocelluloses obtained from wood cellulose fibers.[131] The most commonly used cellulose can be directly taken from plants, like wood and cotton.[139] The cellulose fibers are deconstructed into microfibrils and eventually obtain well-organized CNCs that are known to be piezoelectric.[47] The piezoelectric polarity in CNCs is a result of the polarized glucose units that are linearly aligned through glycosidic linkage in a monoclinic lattice. So far, many experimental and theoretical works have invested the nano- and bulk-scale piezoelectricity in CNCs and their assemblies.[131,140] Csoka et al. manufactured ultrathin CNC films with the typical thickness of 38 nm, and the alignment of CNCs within the films was controlled by a combination of shear and electrical fields (Figure 8b).[132] The effective piezoelectric coefficients d_{25} were measured with the highest value up to 210 pm V^{-1}. Zhai et al. investigated[133] the effective out-of-plane piezoelectric coefficients $d_{33,\text{eff}}$ of cellulose nanofiber films (CNF) via three different methods, corona poling, electric in-plane, and high magnetic field, were measured by using PFM. As shown in Figure 8c, the corona-poling method resulted in the largest piezoresponse with the $d_{33,\text{eff}}$ of 2.31 pm V^{-1}.

Due to the fibrous structure, CNC assemblies typically exhibited a sheet-like structure with in-plane polarizations. Therefore, the shear-type piezoresponses were more commonly observed, and the out-of-plane polarization was usually small. Aligning dipole moments in cellulose chain with CNCs vertically would be geometrically ideal to exhibit a strong out-of-plane piezoelectric performance in bulk form.[134,140] In 2020, Wang et al. fabricated vertically aligned CNC films via a direct current (DC)-assisted confinement cell technology.[134] In this process, the high interfacial energy together with torque induced by shear force from the capillary flow stabilized the vertical alignment of CNC rods with all the dipole moments pointing perpendicular to the film surface (Figure 8d,e). As a result, the PFM measurement found the average piezoelectric coefficient d_{33} reached 19.3 ± 2.9 pm V^{-1}, which was close to the d_{33} of a PVDF film. Besides, the piezoelectricity of cellulose films were also improved by incorporating high-piezoelectric nanofillers such as barium

titanate, zinc oxide, and manganese ferrite.[141–143] While these approaches indeed increased the composite films' piezoelectric responses, the effect was primarily contributed by the fillers, while the cellulose merely served as a supporting matrix.[144–146] Here, we do not consider this type of strategy intrinsic to piezoelectric CNCs and thus not include them in the comparison.

Chitin is another abundant polysaccharide only after cellulose and exists as the major component of marine crustacean shells.[147] Chitin is a long-chain polymer of *N*-acetyl-D-glucosamine and can be deacetylated into poly(D-glucosamine), a well-known derivative chitosan.[148] The monomer structures of chitin and chitosan are shown in Figure 8f. With a structure similar to cellulose, both chitin and chitosan were reported to exhibit piezoelectricity due to their noncentrosymmetric crystal structure. The study of piezoelectricity in chitin dates back to 1975.[149] Recently, driven by the rising interests in piezoelectric natural resources, more studies have been focused on this group of materials.

DFT calculation performed by Kim et al. shows the β-chitin nanofiber has its theoretical overall net polarization along the $[00\bar{1}]$ direction (Figure 8g).[40] Experimentally, the piezoelectric constant of β-rich chitin film was measured by PFM as 3.986 pm V^{-1}. Similar to CNCs, aligning the electrical dipole is essential for the film to show strong piezoelectricity. Given the similar chemistry of both types of materials, some strategies could be shared in their fabrication. Street et al. manufactured chitin films by an air gap electrospinning method and compared its piezoelectricity with collagen and gelatin films fabricated under the same conditions.[136] As shown in Figure 8h, piezoelectric response was greatly enhanced in aligned chitin nanofibers than random chitin nanofibers, and this aligning enhancement is more significant in chitin than the other two samples due to its linear structure. Recently, researchers demonstrated the enhancement of piezoelectricity in chitosan through postcasting neutralization.[135] The $d_{33,\mathrm{eff}}$ obtained from the chitosan film neutralized for 60 min measuring by PFM was 15.56 pm V^{-1} (Figure 8i). Praveen et al. prepared chitosan films with various organic acids and compared d_{33} coefficients of as-prepared chitosan films under varied mechanical pressures.[137] A chitosan film with smooth surface could be obtained from chitosan-formic acid solutions (Figure 8j). The piezoelectricity in chitosan film was stable up to 330 K and had a maximum d_{33} of 18.4 pm V^{-1} under a load of 5 tons (Figure 8k).

What we can find out from these comparisons is that the piezoelectric responses are much stronger in polysaccharide films than those from proteins. The fabrication strategies are also much more developed and understood, so that we can often see large scale films being reported from polysaccharides. This capability allows the demonstration and development of devices from this group of natural piezoelectric biomaterials. Nevertheless, their piezoelectric output is still not noticeably improved from those fabrication approaches. This may be limited by the nature of their molecules, but it did not restrict the increasing number of demonstrations for their applications as a promising green and biodegradable building block for energy harvesting and conversion.

5. BIOMEDICAL APPLICATIONS

Owing to their characteristic biocompatibility and biodegradability,[2,150] natural piezoelectric biomaterials are ideal choices for biomedical applications, particularly for implantable and degradable systems. Compared to the well-developed ceramic or synthetic polymer counter parts, applications of the natural piezoelectric biomaterials are still at a very early stage. However, their intriguing promises are still driving continuous and growing research efforts into this emerging field. Similar to other piezoelectric materials, applications of this group of piezoelectric biomaterials are mostly allocated in mechanical energy harvesting, sensing, and tissue engineering. Here, we focus our discussion on these three directions to demonstrate their application potentials as well as associated challenges.

5.1. Mechanical Energy Harvesting.

Piezoelectric materials have long been used as the fundamental building block for energy conversion between mechanical strain and electricity. This application was substantially extended to a broad range of directions driven by the evolution of nanogenerator (NG) technology, which uses piezoelectric nanomaterials for harvesting mechanical energy from the ambient environment.[9,151] Discoveries of appreciable piezoelectricity from natural biomaterials offered potential possibility for interfacing the NG technology with human beings, serving as a promising alternative to batteries in bioelectronics. The targeted energy sources are mostly focused on regular biomechanical motions such as muscle stretching, breathing, and heart beating.[152] Similar to other wearable and implantable biomedical devices, harvesting mechanical energy from human body particularly stresses biocompatibility and biosafety in addition to their performance. In this regard, although the natural piezoelectric biomaterials have lower performance than their ceramic and synthetic polymer counterparts, they are still the most favorable choices for designing NGs for biomechanical energy harvesting.[48,78,109,110,153,154]

Among the natural piezoelectric biomaterials introduced in this review, polysaccharides, particularly cellulose-based materials, are mostly investigated for NG development. This may be largely attributed to the abundant, diverse, and ecofriendly cellulose raw materials. However, as mentioned in the materials discussion, the assembly of piezoelectric CNC crystals is fairly challenging over a practically large area. Therefore, most reported cellulose-based NGs were built on composites with other piezoelectric materials or through other mechanisms, such as the triboelectric effect. As this application strategy has been covered extensively in recent reviews,[129,130,139,155,156] here we will not go into further details on this directly. However, we want to point out that the piezoelectric effect is a bulk/volume-related property and is more significant in charge generation compared to the triboelectric effect. This feature may place piezoelectricity at a more desirable position for biomedical applications, where electric current is usually considered the most critical factor. Therefore, there is still plenty of room and potential for the application of the true piezoelectric effect in CNC assemblies, if long-range ordered structures can be realized in bulk without jeopardizing their mechanical integrity.

Aside from cellulose, amino acids are another emerging group of piezoelectric biomaterials that recently demonstrated substantial progress in NG applications. The capability of

growing large-scale crystals of amino acids allowed fabrication of NG devices for practical applications. Besides, the smallsized molecule and high concentration of hydrophilic groups of amino acids enable fast dissolution of their crystalline phases in body fluids. Thus, they typically show good biodegradability. The fast dissolution allows a better control of the device's lifetime merely by the packaging layer and ensures immediate termination of the device function when the package layer is degraded. A representative example was offered by Yang et al. in their recent development of PLA-packaged glycine-PVA NGs. The devices were implanted in adult Sprague–Dawley rats to test the ability of energy harvesting at different areas.[37] Figure 9a showed the device attached under the thigh produced a stable peak-to-peak voltage (V_{pp}) of >150 mV from quadriceps femoris muscle movement during leg stretching. Another device in the chest generated a V_{pp} of >20 mV from pectoralis major muscle in response to rat respiration. The unpackaged devices could completely degrade in the body environment <1 day of implantation without any inflammation in the body.

Another interesting strategy in biomaterial-based NG development is to leverage natural structures directly from animals or plants, as directed by the understanding of the piezoelectricity of their fundamental building blocks. This strategy can bypass or minimize the complex or yet-to-realize assembly processes to achieve desired polarization alignment over a large area. Ghosh et al. fabricated a high-performance NGs from a natural collagen-containing material, fish swim bladder, with oriented collagen nanofibrils.[157] An open-circuit voltage up to 10 V and a short-circuit current of 51 nA were obtained when the device was deflected by finger compression (Figure 9b,c). The energy conversion efficiency of ~0.3% was claimed from this device for mechanical energy harvesting. Another example of collagen containing biomaterial for energy harvesting is porous eggshell membrane (ESM), a thin layer in-between the calcified eggshell and albumen proteins of eggs (Figure 9d), which comprises different types of collagen (I, V, and X) and other proteins. Collagen I is the major component of both outer and inner membrane fibers,[161] which is believed to be the main component contributing to the piezoelectricity in ESM. Karan et al. demonstrated a flexible NG using a ESM as the piezoelectric component.[158] The output voltages generated from the ESM-NG monotonically increased from ~6 V to ~27 V as the applying pressure rose from 8 to 90 kPa and then saturated after 90 kPa (Figure 9e). Maiti et al. reported a NG made from untreated onionskin with self-aligned cellulose fibers (Figure 9f).[159] The onionskin-based NG displayed an output voltage and current of 18 V and 166 nA by finger tapping. Hoque et al. fabricated a piezoelectric nanogenerator based on chitin nanofibers extracted from a crab cell with the calculated piezoelectric coefficient d_{33}= 9.49 Pc N^{-1}.[162]

It is known that the ordering of large molecules in natural systems are generally imperfect, as amorphous or different molecules are always involved. Therefore, the lower piezoelectric effect can be expected from those systems compared to perfectly ordered piezoelectric biocrystals. Given the easy access and facile process of these natural materials, some sacrificing of performance may still be acceptable for applications where energy conversion efficiency is not the major concern. We also noted that the voltage output of those devices was relatively high, while the input mechanical energy was not clearly specified. These outputs already reached those that can be produced by commercial piezoelectric materials. Based on the device geometry, we suspect that some of the measurements may also include other surface charge contributions. Although hybrid NGs incorporating both piezoelectric

and triboelectric effects have been reported as a successful strategy to improve the overall output,[163] it is still essential to identify the contributions from different mechanisms to establish a reliable materials property relationship.

Viruses have also been considered as promising building blocks for energy harvesting due to their potential tunability of dipole moment from genetic and chemical modification.[38] Lee et al. developed the virus-based NG with a self-assembled M13 phage film that produced up to 6 Na of current and 400 Mv of potential.[48] The piezoelectric performance of phage-based PENG was further improved through the alignment of phages.[121,122] Recently, Yan et al. explored the separation of the piezoelectric and flexoelectric effects from the electric outputs generated by phage-based NG.[160] The quadrant electrode NG in Figure 9h along with nematically organized M13 bacteriophage provided the comprehensive piezoelectric coefficients. The short-circuit currents increased linearly with applied loads from 20 to 80 N (Figure 9i) and reached up to 43.5 Na for axial measurement. This study helped to identify the contributions from multiple mechanistic origins on electric polarization, providing an in-depth understanding of electrical outputs and enabling better designs of advanced devices for energy harvesting. In addition to the output quantification, there are no practical devices being demonstrated so far. Again, large-scale assembly and manufacturing are still the main challenges. Since it is much more costly to obtain the raw virus materials, their application may be more suitable for nanoscale surface piezoelectric functions, such as sensors or surface acoustic wave transduction.

5.2. Sensors.

Pressure or force sensing is another common application direction of the piezoelectric effect. A self-powered mechanical sensor could be achieved by nanogenerators directly serving as power sources.[164] Unlike energy harvesting, sensing emphasizes more on monotonic signal correlation instead of high energy output. Piezoelectric biomaterials, naturally with great flexibility and relatively low-performance, could be more suitable for biomedical sensing applications. For example, low-piezoelectric CNF films were able to be used as force sensors, although the randomly oriented CNF made it unsuitable for mechanical energy harvesting (Figure 10a,b).[47] Enhanced piezoelectricity was introduced to chitosan films by improved crystallographic alignment via a controlled solvent casting technique and postcasting treatment.[135] This advancement enabled the development of flexible ultrasound transducers based on chitosan with a high sensitivity of 80 mV kPa^{-1} and working in a range of few MHz. The physiological signal monitoring could also be achieved by sensors based on piezoelectric biomaterials.[165,166] For example, a fish-skin-based self-powered piezoelectric sensor was demonstrated to monitor small physiological signals such as arterial pulses, vocal cord vibration, and gentle wrist movements.[167]

The piezoelectric effect also allows molecular sensing of specific biomolecules via monitoring the resonance frequency change caused by a mass bound on the sensor surface.[169] Recently, Li et al. developed a biosensor for quantification of immunoglobulin Y (igY) by combining carboxymethyl chitosan hydrogel with quartz crystal microbalance (Figure 10c). The sensing performances were evaluated in terms of response time, detection limit, and selectivity. As shown in Figure 10d, frequency shifts were recorded after

the buffer injection carrying different IgY. The obtained data were fitted to Langmuir isotherm model, and the estimated detection limit was 65 ng/mL at 240 s. Given that the concentration level of IgY in blood is about 5–6 mg/mL, the established protocol in this work was effective for quantification in highly diluted buffer. In Figure 10e, the sensor responses of two other proteins, bovine serum albumin (BSA) and lysozyme, with different isoelectric points suggesting different adsorption behavior were measured to demonstrate the sensor selectivity. There was negligible response upon injection of BSA and lysozyme, confirming the resistance to nonspecific binding.[168] The sensing mechanism of piezoelectric biomaterials has been extended to humidity. Vivekananthan et al. coated a piezoelectric collagen nanofibril biopolymer on to a cotton fabric as a sensor to measure various percentages of relative humidity (Figure 10f).[97] The humidity sensor showed a linear response with a good sensitivity in the range of 50–90% relative humidity. In principle, the sensing mechanism is not different from other piezoelectric sensors. However, enabling the same function using these natural piezoelectric biomaterials may allow for integrating essential sensing or monitoring function in biomedical devices. Realizing the degradable biosensor may also become possible.

5.3. Tissue Engineering.

Owing to their excellent biocompatibility, natural biomaterials such as collagen and chitosan have been intensively studied to develop tissue scaffolds. In this application direction, most efforts were devoted to the investigation of cellular behaviors with artificial tissue scaffolds such as inflammatory response and the optimization of mechanical and structural features of scaffolds.[27,170–174] An intriguing add-on strategy to facilitate tissue growth is to use electrical stimulation (ES), which is known to be able to promote cell proliferation and differentiation.[175] The discovery of piezoelectricity in bone inspired research into the role of biopiezoelectricity in tissue regeneration and the development of biomimetic tissue scaffolds for self-healing environment in tissues.[24,27,176]

Nowadays, the fundamental understanding and implementation of piezoelectricity in biomaterials on regulating cell activities and promoting cell growth emerged at the cutting edge of tissue engineering.[178–181] Fernandez-Yague et al. demonstrated the effect of collagen-analogue-based piezobioelectric devices on the dynamic response of tendon cells by modulating the expression of ion channels and specific tissue regeneration signaling pathways.[176] The impact from a standard moderate treadmill running protocol (MTR) on tissue-repair processes was evaluated in a rat achilles acute injury model (Figure 11a). Significant increases in tissue organization assessed by level of fiber orientation and a decrease in calcifications assessed by presence of glycosaminoglycans were observed in tendon tissues treated with piezoelectric scaffold (Figure 11b,c), indicating the potential of implantable piezo-bioelectric devices in postinjury mechanotherapy for tendon regeneration and self-powered healing. Moreover, Du et al. came up with the synergetic interplay between external ES and piezoelectric voltage for nerve tissue engineering.[177] The PEDOT/chitosan nanofibers with a shell–core structure were fabricated by integrating the electrospinning method and recrystallization. As shown in Figure 11d–f, PEDOT/chitosan PEDOT/chitosan nanofibers boosted the growth and neurites development of brain neuroglioma cells (BNCs) through the piezoelectric charges from the substrate.

The PEDOT/chitosan nanofibers were considered as promising materials for implantable electroactive scaffolds in biomedical applications. Besides, cellulose is another natural piezoelectric polymer that can be a suitable candidate for tissue engineering due to its superior hydrophilicity and good mechanical strength.[27] Zaborowska et al. prepared microporous bacterial cellulose scaffolds with improved cell seeding and migration of MC3T3-E1 osteoprogenitor cells, offering an additional option for bone regeneration.[182]

Applying piezoelectric natural material for ES-facilitated tissue engineering has a few obvious advantages, particularly from the biocompatibility perspective. It may effectively address several clinical limitations for adopting ES treatment, including the infection risk of electrodes, potential nonspecific off-target effects, technical complications of ES set up, and low efficiency with small working area.[28,176,183,184] Although promising, research in this area is still at the very early stage. One major uncertainty is the characteristics of ES imposed by the materials. In principle, piezoelectric polarization requires mechanical strain to activate, and the resulting ES amplitude is dependent on the level of strain received. In the application demonstration, some systems have dynamic strain incorporated, but some systems do not. In the cases where no dynamic strains were involved, the polarization may be induced by the intrinsic permanent dipoles, i.e., ferroelectricity, which may be considered equivalent to a piezoelectric material subjecting to a constant strain. Nevertheless, if dynamic strains were applied, like those NG application conditions, the ES pattern would be completely different, i.e., the interfacial charge would be constantly refreshed. It is therefore critical to understand the natural electrical signal from the piezoelectric biomaterials based on their implementation environment when researchers are trying to understand and analyze the biological influences of their ES effect.

6. CONCLUSION AND PERSPECTIVES

In this review, we systematically reviewed the most recent research progresses in natural piezoelectric biomaterials. Five major types of natural piezoelectric biomaterials including amino acids, peptides, proteins, virus, and polysaccharides are discussed. Here, we focused on their piezoelectric properties related to their structures and fabrication strategies to achieve desired piezoelectric phases. We compared and analyzed their piezoelectric performance and particularly commented on the approaches to improve their output and reliability and summarized in Table 1 for better comparison. Their applications as biomedical devices, including mechanical energy harvesting, sensing, and tissue engineering are also discussed. Despite the growing research interests and efforts in this field, the development and applications of natural piezoelectric biomaterials are still at a very early stage. Compared to other well-studied piezoelectric materials, they are still facing several critical challenges for them to move toward practical and scalable devices.

First, a fundamental understanding of the piezoelectricity in biomaterials is still largely lacking at the molecular level.[48,185] Unlike inorganic piezoelectric materials, the polarization in biomaterials typically originated from the molecular dipoles. Their organization and alignment are rather complicated compared to inorganic crystals. In addition, these piezoelectric biomaterials normally have multiple polymorphs with a relatively low crystal symmetry. The piezoelectric phase has aligned dipoles and is

normally high energy and maybe metastable. Therefore, complicity in understanding and predicting the piezoelectric property is always introduced by the nonideal heterogeneity or inhomogeneity of the material. As we discussed in this review, theoretical calculations were typically built on simple and idealized models. Discrepancies were commonly shown among experiments as well as between the experimental results and the predictions.[24,186] Therefore, it is crucial to build reliable connections between materials' structure, phase, and chemistry with their piezoelectric properties. Due to the relatively sensitive chemistry of these biomaterials, high-energy electron beams can easily and quickly damage the lattice. This is the reason that we do not often see high-quality and comprehensive lattice images from the biomaterial crystals. This limitation seriously restricted researchers from establishing a reliable correction between the piezoelectricity and their structures both experimentally and theoretically. As cryo-TEM is a more and more popular tool for materials characterization, we expect this advanced technique may soon bring some groundbreaking understandings in the materials science of piezoelectric biomaterials.

Second, the piezoelectricity is generally low for the natural piezoelectric biomaterials. As previously discussed (Table 1), the piezoelectric coefficients of this group of materials are typically below 10 pC/N. Although the high end of their piezoelectric coefficients is comparable to that of some synthetic polymers, they are still far from the commonly used inorganic piezoelectric materials.[28] In addition, their structural nature typically generates high piezoelectricity in a shear mode. Macroscopically, the often random orientation of their crystal polarization domains usually leads to the reduction or cancellation of net polarization. All these limitations make their practical applications rather challenging. In most recent publications, the reported performances of proof-of-concept demonstrations were still marginal. We envision there are two levels of improvement that may lead to revolutionary advancement in addressing this challenge. On the macroscopic level, effective alignment methods and optimized design of structures are a promising strategy to improve the piezoelectric performances. As the poling electric field is much higher in biocrystals than those required for ceramics, self-assembly approaches are much more preferred to create automatically aligned polarization domain orientation. As demonstrated in Yang's work,[37] interface control can be an effective strategy for domain alignment over a large scale. This may be particularly useful for the biomolecules that usually have specific functional groups available for selective bonding. On the molecular level, it is extremely attractive to modulate the biomaterial molecules to improve the intrinsic piezoelectric polarization. All four types of natural piezoelectric biomaterials possess rich functional groups as well as the capability of incorporating with other ions.[187–190] This property allows researchers to introduce additional charges or dipoles to the molecular assembly and further enhance the overall polarization. This strategy may also improve the transverse piezoelectric coefficients, e.g., d_{33}, to make the crystals more application adaptable.

Third, large-scale synthesis or manufacturing is also essential for practical applications. We noted that currently most research on piezoelectric biomaterials is still at a very small scale for fundamental property studies or proof-of-concept demonstrations. The materials synthesized and studied were primarily nanoparticles, nanowires, or 2D nanosheets. However, most applications of piezoelectric materials, such as NGs, sensors, and scaffolds, all require bulk-scale material building blocks. It is necessary to develop effective methods

for mass production of high-quality piezoelectric biomaterials for the development of practical devices. While this requirement appears to be rather engineering based, the science for scalable synthesis needs to be fundamentally addressed. For example, how to control the phase uniformity on a large scale; how to transfer the molecular-scale interactions for polarization control to millimeter scale and beyond; to what level that our observed microscale self-assemble can still hold; what continuous manufacturing techniques can be adapted to the synthesis approaches? Of course, many more fundamental questions may arise for specific techniques or material systems. Emerging technologies, such as additive manufacturing, are also expected to provide opportunities in materials preparation and device fabrication. We may further look into guidance or establish more informative blue prints for materials manufacturing by leveraging state-of-the-art data science and machine learning approaches.

In general, the natural piezoelectric materials hold substantial potential as an emerging group of functional materials for electromechanical applications. Their natural characteristics place them at an extremely advantageous position for biomedical applications with incomparable biocompatibility, biosafety, and environmental sustainability. We do not expect the challenges that we outlined above might diminish their potential. Instead, they are associated with substantial research opportunities that will bring in many groundbreaking fundamental understandings and engineering innovations. We anticipate the group of natural piezoelectric biomaterials will soon stand out as a promising interdisciplinary subfield at the junction between material science and biomedical engineering.

ACKNOWLEDGMENTS

This publication was supported by the National Science Foundation DMR-2114931 and the National Heart, Lung, and Blood Institute of the National Institutes of Health under award number R01HL157077.

REFERENCES

(1). Katzir S In The Beginnings of Piezoelectricity; Springer: Dordrecht, 2006; pp 15–64.

(2). Shin D-M; Hong SW; Hwang Y-H Recent advances in organic piezoelectric biomaterials for energy and biomedical applications. Nanomaterials 2020, 10, 123. [PubMed: 31936527]

(3). Jaffe B; Roth R; Marzullo S Piezoelectric properties of lead zirconate-lead titanate solid-solution ceramics. J. Appl. Phys 1954, 25, 809–810.

(4). Berlincourt D; Jaffe H Elastic and piezoelectric coefficients of single-crystal barium titanate. Phys. Rev 1958, 111, 143.

(5). Acosta M; et al. BaTiO3-based piezoelectrics: Fundamentals, current status, and perspectives. Applied Physics Reviews 2017, 4, 041305.

(6). Collins E; Pantoya M; Neuber AA; Daniels M Piezoelectric ignition of nanocomposite energetic materials. Journal of Propulsion and Power 2014, 30, 15–18.

(7). Choi W; et al. Enhanced sensitivity of piezoelectric pressure sensor with microstructured polydimethylsiloxane layer. Appl. Phys. Lett 2014, 104, 123701.

(8). Dosch JJ; Inman DJ; Garcia E A self-sensing piezoelectric actuator for collocated control. Journal of Intelligent material systems and Structures 1992, 3, 166–185.

(9). Wang ZL; Song. J. Piezoelectric nanogenerators based on zinc oxide nanowire arrays. Science 2006, 312, 242–246. [PubMed: 16614215]

(10). Xu S; Hansen BJ; Wang ZL Piezoelectric-nanowireenabled power source for driving wireless microelectronics. Nat. Commun 2010, 1, 93. [PubMed: 20981021]

(11). Ramadan KS; Sameoto D; Evoy S A review of piezoelectric polymers as functional materials for electromechanical transducers. Smart Materials and Structures 2014, 23, 033001.

(12). Chorsi MT; et al. Piezoelectric biomaterials for sensors and actuators. Adv. Mater 2019, 31, 1802084.

(13). Jain A; Prashanth KJ; Sharma AK; Jain A; Rashmi PN Dielectric and piezoelectric properties of PVDF/PZT composites: A review. Polym. Eng. Sci 2015, 55, 1589–1616.

(14). Martin A Tribo-electricity in wool and hair. Proc. Phys. Soc 1941, 53, 186.

(15). Fukada E Piezoelectricity as a fundamental property of wood. Wood Science and Technology 1968, 2, 299–307.

(16). Bassett CAL; Becker RO Generation of electric potentials by bone in response to mechanical stress. Science 1962, 137, 1063–1064. [PubMed: 13865637]

(17). Hastings G; Mahmud F Electrical effects in bone. Journal of biomedical engineering 1988, 10, 515–521. [PubMed: 3070168]

(18). Williams WS; Breger L Piezoelectricity in tendon and bone. J. Biomech 1975, 8, 407–413. [PubMed: 1206043]

(19). Athenstaedt H; Claussen H; Schaper D Epidermis of human skin: pyroelectric and piezoelectric sensor layer. Science 1982, 216, 1018–1020. [PubMed: 6177041]

(20). Bassett CAL; Pawluk RJ Electrical behavior of cartilage during loading. Science 1972, 178, 982–983. [PubMed: 5084665]

(21). Fukada E; Hara K Piezoelectric effect in blood vessel walls. J. Phys. Soc. Jpn 1969, 26, 777–780.

(22). Shamos MH; Lavine LS Piezoelectricity as a fundamental property of biological tissues. Nature 1967, 213, 267–269. [PubMed: 6030604]

(23). Bassett CAL Biologic significance of piezoelectricity. Calcified tissue research 1967, 1, 252–272.

(24). Lay R; Deijs GS; Malmström J The intrinsic piezoelectric properties of materials–a review with a focus on biological materials. RSC Adv. 2021, 11, 30657–30673. [PubMed: 35498945]

(25). Kim D; et al. Biomolecular piezoelectric materials: from amino acids to living tissues. Adv. Mater 2020, 32, 1906989.

(26). Yasuda I Electrical callus and callus formation by electret. Clin. Orthop. Relat. Res 1977, 124, 53–56.

(27). Khare D; Basu B; Dubey AK Electrical stimulation and piezoelectric biomaterials for bone tissue engineering applications. Biomaterials 2020, 258, 120280. [PubMed: 32810650]

(28). Kapat K; Shubhra QT; Zhou M; Leeuwenburgh S Piezoelectric Nano-Biomaterials for Biomedicine and Tissue Regeneration. Adv. Funct. Mater 2020, 30, 1909045.

(29). Ahn AC; Grodzinsky AJ Relevance of collagen piezoelectricity to “Wolff’s Law”: A critical review. Medical engineering & physics 2009, 31, 733–741. [PubMed: 19286413]

(30). Guerin S; Syed TA; Thompson D Deconstructing collagen piezoelectricity using alanine-hydroxyproline-glycine building blocks. Nanoscale 2018, 10, 9653–9663. [PubMed: 29757342]

(31). Jiang P; et al. Electromechanical coupling of murine lung tissues probed by piezoresponse force microscopy. ACS Biomaterials Science & Engineering 2017, 3, 1827–1835. [PubMed: 33429664]

(32). Coste B; et al. Piezo1 and Piezo2 are essential components of distinct mechanically activated cation channels. Science 2010, 330, 55–60. [PubMed: 20813920]

(33). Ranade SS; et al. Piezo2 is the major transducer of mechanical forces for touch sensation in mice. Nature 2014, 516, 121–125. [PubMed: 25471886]

(34). Chesler AT; et al. The role of PIEZO2 in human mechanosensation. New England Journal of Medicine 2016, 375, 1355–1364. [PubMed: 27653382]

(35). Li C; et al. Design of biodegradable, implantable devices towards clinical translation. Nature Reviews Materials 2020, 5, 61–81.

(36). Someya T; Bao Z; Malliaras GG The rise of plastic bioelectronics. Nature 2016, 540, 379–385. [PubMed: 27974769]

(37). Yang F; et al. Wafer-scale heterostructured piezoelectric bioorganic thin films. Science 2021, 373, 337–342. [PubMed: 34437153]

(38). Li J; Long Y; Yang F; Wang X Degradable piezoelectric biomaterials for wearable and implantable bioelectronics. Curr. Opin. Solid State Mater. Sci 2020, 24, 100806. [PubMed: 32313430]

(39). Nguyen T Degradation of poly [vinyl fluoride] and poly [vinylidene fluoride]. Polym. Rev 1985, 25, 227–275.

(40). Kim K; et al. Biodegradable, electro-active chitin nanofiber films for flexible piezoelectric transducers. Nano Energy 2018, 48, 275–283.

(41). Ahmad F; Akmal MM; Amran A et al. Characterization of chitosan from extracted fungal biomass for piezoelectric application. Proceedings from the IOP Conference Series: Materials Science and Engineering, 26th Regional Symposium on Chemical Engineering, Kuala Lumpur, Malaysia, October 30–31, 2019; Hussain M, Keong T, et al. Eds.; IOP publishing: Philadelphia, PA, 2020; p 778.

(42). Guerin S; et al. Control of piezoelectricity in amino acids by supramolecular packing. Nature materials 2018, 17, 180–186. [PubMed: 29200197]

(43). Nguyen V; Zhu R; Jenkins K; Yang R Self-assembly of diphenylalanine peptide with controlled polarization for power generation. Nat. Commun 2016, 7, 13566. [PubMed: 27857133]

(44). Fukada E; Yasuda I Piezoelectric effects in collagen. Jpn. J. Appl. Phys 1964, 3, 117.

(45). Yucel T; Cebe P; Kaplan DL Structural origins of silk piezoelectricity. Adv. Funct. Mater 2011, 21, 779–785. [PubMed: 23335872]

(46). Ando Y; Fukada E; Glimcher MJ Piezoelectricity of chitin in lobster shell and apodeme. Biorheology 1977, 14, 175–179. [PubMed: 912046]

(47). Rajala S; et al. Cellulose nanofibril film as a piezoelectric sensor material. ACS Appl. Mater. Interfaces 2016, 8, 15607–15614. [PubMed: 27232271]

(48). Lee BY; et al. Virus-based piezoelectric energy generation. Nature Nanotechnol. 2012, 7, 351–356. [PubMed: 22581406]

(49). Hosseini ES; Manjakkal L; Shakthivel D; Dahiya R Glycine—chitosan-based flexible biodegradable piezoelectric pressure sensor. ACS Appl. Mater. Interfaces 2020, 12, 9008–9016. [PubMed: 32011853]

(50). Zaszczynska A; Sajkiewicz P; Gradys A Piezoelectric scaffolds as smart materials for neural tissue engineering. Polymers 2020, 12, 161. [PubMed: 31936240]

(51). Jacob J; More N; Kalia K; Kapusetti G Piezoelectric smart biomaterials for bone and cartilage tissue engineering. Inflammation Regener. 2018, 38, 2.

(52). Fukada E Piezoelectricity of natural biomaterials. Ferroelectrics 1984, 60, 285–296.

(53). Yuan H; Lei T; Qin Y; He J-H; Yang R Design and application of piezoelectric biomaterials. J. Phys. D: Appl. Phys 2019, 52, 194002.

(54). Vasilescu D; Cornillon R; Mallet G Piezoelectric resonances in amino-acids. Nature 1970, 225, 635–635. [PubMed: 5413369]

(55). Lemanov V; Popov S; Pankova G Piezoelectricity in protein amino acids. Phys. Solid State 2011, 53, 1191–1193.

(56). Xu Q; et al. Construction of Bio-Piezoelectric Platforms: From Structures and Synthesis to Applications. Adv. Mater 2021, 33, 2008452.

(57). Albrecht G; Corey RB The crystal structure of glycine. J. Am. Chem. Soc 1939, 61, 1087–1103.

(58). Dishon S; et al. Surface piezoelectricity and pyroelectricity in centrosymmetric materials: A case of α-glycine. Materials 2020, 13, 4663. [PubMed: 33086709]

(59). Iitaka Y Crystal structure of β-glycine. Nature 1959, 183, 390–391.

(60). Iitaka Y The crystal structure of γ-glycine. Acta Crystallogr. 1958, 11, 225–226.

(61). Goes J; Figueiro S; De Paiva J; Sombra A Piezoelectric and dielectric properties of collagen films. physica status solidi (a) 1999, 176, 1077–1083.

(62). Heredia A; et al. Nanoscale ferroelectricity in crystalline γ-glycine. Adv. Funct. Mater 2012, 22, 2996–3003.

(63). Ueberschlag P PVDF piezoelectric polymer. Sensor review 2001, 21, 118–126.

(64). Murayama N; Nakamura K; Obara H; Segawa M The strong piezoelectricity in polyvinylidene fluroide (PVDF). Ultrasonics 1976, 14, 15–24.

(65). Kholkin A; Amdursky N; Bdikin I; Gazit E; Rosenman G Strong piezoelectricity in bioinspired peptide nanotubes. ACS Nano 2010, 4, 610–614. [PubMed: 20131852]

(66). Gao J; Xue D; Liu W; Zhou C; Ren X Recent Progress on BaTiO3-Based Piezoelectric Ceramics for Actuator Applications. Actuators 2017, 6, 24.

(67). Beeby SP; Tudor MJ; White N Energy harvesting vibration sources for microsystems applications. Measurement science and technology 2006, 17, R175.

(68). Ferrari ES; Davey RJ; Cross WI; Gillon AL; Towler CS Crystallization in polymorphic systems: the solution-mediated transformation of β to α glycine. Cryst. Growth Des 2003, 3, 53–60.

(69). Isakov D; et al. In situ observation of the humidity controlled polymorphic phase transformation in glycine microcrystals. Cryst. Growth Des 2014, 14, 4138–4142.

(70). Isakov D; et al. Production of polar β-glycine nanofibers with enhanced nonlinear optical and piezoelectric properties. Cryst. Growth Des. 2011, 11, 4288–4291.

(71). Sui J; Li J; Gu L; Schmidt CA; Zhang Z; Shao Y; Gazit E; Gilbert PUPA; Wang X Orientation-Controlled Crystallization of γ-Glycine Films with Enhanced Piezoelectricity. J. Mater. Chem. B 2022, 10, 6958. [PubMed: 35971914]

(72). Kobiakov I Elastic, piezoelectric and dielectric properties of ZnO and CdS single crystals in a wide range of temperatures. Solid State Commun. 1980, 35, 305–310.

(73). Zelenovskii PS; Vasileva DS; Vasilev SG; Kopyl S; Kholkin A Ferroelectricity in glycine: A mini-review. Frontiers in Materials 2022, 9, 918890.

(74). Seyedhosseini E; et al. Self-assembly of organic ferroelectrics by evaporative dewetting: A case of β-Glycine. ACS Appl. Mater. Interfaces 2017, 9, 20029–20037. [PubMed: 28534399]

(75). Bystrov V; et al. Bioferroelectricity in nanostructured glycine and thymine: molecular modeling and ferroelectric properties at the nanoscale. Ferroelectrics 2015, 475, 107–126.

(76). Bystrov V; et al. Glycine nanostructures and domains in betaglycine: computational modeling and PFM observations. Ferroelectrics 2016, 496, 28–45.

(77). Hu P; et al. Bioferroelectric properties of glycine crystals. J. Phys. Chem. Lett 2019, 10, 1319–1324. [PubMed: 30776247]

(78). Lee J-H; et al. Diphenylalanine peptide nanotube energy harvesters. ACS Nano 2018, 12, 8138–8144. [PubMed: 30071165]

(79). Yang J; et al. Three-Dimensional Printing of Self-Assembled Dipeptides. ACS Appl. Mater. Interfaces 2021, 13, 20573–20580. [PubMed: 33896166]

(80). Zelenovskii PS; et al. 2D Layered Dipeptide Crystals for Piezoelectric Applications. Adv. Funct. Mater 2021, 31, 2102524.

(81). Yuan H; Han P; Tao K; Liu S; Gazit E; Yang R Piezoelectric peptide and metabolite materials. Research 2019, 2019, 9025939. [PubMed: 31912048]

(82). Ryan K; et al. Nanoscale piezoelectric properties of selfassembled fmoc–FF peptide fibrous networks. ACS Appl. Mater. Interfaces 2015, 7, 12702–12707. [PubMed: 25994251]

(83). Tao K; et al. Bioinspired stable and photoluminescent assemblies for power generation. Adv. Mater 2019, 31, 1807481.

(84). Tao K; et al. Stable and optoelectronic dipeptide assemblies for power harvesting. Mater. Today 2019, 30, 10–16.

(85). Tabata Y; Takagaki K; Uji H; Kimura S Piezoelectric property of bundled peptide nanotubes stapled by bis-cyclic-β-peptide. Journal of Peptide Science 2019, 25, No. e3134.

(86). Tao K; Makam P; Aizen R; Gazit E Self-assembling peptide semiconductors. Science 2017, 358, No. eaam9756.

(87). Basavalingappa V; et al. Diphenylalanine-derivative peptide assemblies with increased aromaticity exhibit metal-like rigidity and high piezoelectricity. ACS Nano 2020, 14, 7025–7037. [PubMed: 32441511]

(88). Anderson J; Lake PT; McCullagh M Initial Aggregation and Ordering Mechanism of Diphenylalanine from Microsecond All-Atom Molecular Dynamics Simulations. J. Phys. Chem. B 2018, 122, 12331–12341. [PubMed: 30511861]

(89). Guo C; Luo Y; Zhou R; Wei G Probing the self-assembly mechanism of diphenylalanine-based peptide nanovesicles and nanotubes. ACS Nano 2012, 6, 3907–3918. [PubMed: 22468743]

(90). Vasilev S; et al. Piezoelectric properties of diphenylalanine microtubes prepared from the solution. J. Phys. Chem. Solids 2016, 93, 68–72.

(91). Nguyen V; Jenkins K; Yang R Epitaxial growth of vertically aligned piezoelectric diphenylalanine peptide microrods with uniform polarization. Nano Energy 2015, 17, 323–329.

(92). Sun B; et al. Directed self-assembly of dipeptide single crystal in a capillary. ACS Nano 2018, 12, 1934–1939. [PubMed: 29337528]

(93). Safaryan S; et al. Diphenylalanine-based microribbons for piezoelectric applications via inkjet printing. ACS Appl. Mater. Interfaces 2018, 10, 10543–10551. [PubMed: 29498259]

(94). Arnon ZA; Vitalis A; Levin A; Michaels TCT; Caflisch A; Knowles TPJ; Adler-Abramovich L; Gazit E Dynamic microfluidic control of supramolecular peptide self-assembly. Nat. Commun 2016, 7, 13190. [PubMed: 27779182]

(95). Romanyuk K; et al. Piezoactive dense diphenylalanine thin films via solid-phase crystallization. Applied Materials Today 2022, 26, 101261.

(96). Yuan H; et al. Peptide Coassembly to Enhance Piezoelectricity for Energy Harvesting. ACS Appl. Mater. Interfaces 2022, 14, 6538–6546. [PubMed: 35089003]

(97). Vivekananthan V; et al. Biocompatible collagen nanofibrils: an approach for sustainable energy harvesting and battery-free humidity sensor applications. ACS Appl. Mater. Interfaces 2018, 10, 18650–18656. [PubMed: 29742894]

(98). Erdmann RS; Wennemers H Importance of ring puckering versus interstrand hydrogen bonds for the conformational stability of collagen. Angew. Chem 2011, 123, 6967–6970.

(99). Cartwright VF; Brown CP Hierarchical Piezoresponse in Collagen. Advanced Materials Technologies 2022, 7, 2101166.

(100). Minary-Jolandan M; Yu M-F Uncovering nanoscale electromechanical heterogeneity in the subfibrillar structure of collagen fibrils responsible for the piezoelectricity of bone. ACS Nano 2009, 3, 1859–1863. [PubMed: 19505115]

(101). Denning D; et al. Piezoelectricity in collagen type II fibrils measured by scanning probe microscopy. J. Appl. Phys 2014, 116, 066818.

(102). Ghosh SK; Mandal D High-performance bio-piezoelectric nanogenerator made with fish scale. Appl. Phys. Lett 2016, 109, 103701.

(103). Bella J; Berman HM Crystallographic evidence for Cα–H… O= C hydrogen bonds in a collagen triple helix. Journal of molecular biology 1996, 264, 734–742. [PubMed: 8980682]

(104). Fukada E; Yasuda I On the piezoelectric effect of bone. Journal of the physical society of Japan 1957, 12, 1158–1162.

(105). Marino AA; Becker RO; Soderholm SC Origin of the piezoelectric effect in bone. Calcified tissue research 1971, 8, 177–180. [PubMed: 5145213]

(106). Denning D; Paukshto MV; Habelitz S; Rodriguez BJ Piezoelectric properties of aligned collagen membranes. Journal of Biomedical Materials Research Part B: Applied Biomaterials 2014, 102, 284–292. [PubMed: 24030958]

(107). Chae I; Jeong CK; Ounaies Z; Kim SH Review on electromechanical coupling properties of biomaterials. ACS Applied Bio Materials 2018, 1, 936–953.

(108). Denning D; et al. Piezoelectric tensor of collagen fibrils determined at the nanoscale. ACS Biomaterials Science & Engineering 2017, 3, 929–935. [PubMed: 33429565]

(109). Karan SK; et al. Nature driven spider silk as high energy conversion efficient bio-piezoelectric nanogenerator. Nano Energy 2018, 49, 655–666.

(110). Sencadas V; et al. Electroactive properties of electrospun silk fibroin for energy harvesting applications. Nano Energy 2019, 66, 104106.

(111). Liu Y; et al. Ferroelectric switching of elastin. Proc. Natl. Acad. Sci. U. S. A 2014, 111, E2780–E2786. [PubMed: 24958890]

(112). Veronica A; Hsing I. m. An Insight into Tunable Innate Piezoelectricity of Silk for Green Bioelectronics. ChemPhysChem 2021, 22, 2266–2280. [PubMed: 34423508]

(113). Rockwood DN; et al. Materials fabrication from Bombyx mori silk fibroin. Nature protocols 2011, 6, 1612–1631. [PubMed: 21959241]

(114). Valluzzi R; Gido SP; Zhang W; Muller WS; Kaplan DL Trigonal crystal structure of Bombyx mori silk incorporating a threefold helical chain conformation found at the air-water interface. Macromolecules 1996, 29, 8606–8614.

(115). Fukada E On the piezoelectric effect of silk fibers. J. Phys. Soc. Jpn 1956, 11, 1301A–1301A.

(116). Pasquali-Ronchetti I; Baccarani-Contri M; Fornieri C; Mori G; Quaglino D Jr, Structure and composition of the elastin fibre in normal and pathological conditions. Micron 1993, 24, 75–89.

(117). Liu Y; et al. Glucose suppresses biological ferroelectricity in aortic elastin. Physical review letters 2013, 110, 168101. [PubMed: 23679639]

(118). Stapleton A; et al. Converse piezoelectricity and ferroelectricity in crystals of lysozyme protein revealed by piezoresponse force microscopy. Ferroelectrics 2018, 525, 135–145.

(119). Stapleton A; et al. The direct piezoelectric effect in the globular protein lysozyme. Appl. Phys. Lett 2017, 111, 142902.

(120). Stapleton A; et al. Pyroelectricity in globular protein lysozyme films. J. Appl. Phys 2018, 123, 124701.

(121). Shin D-M; et al. Bioinspired piezoelectric nanogenerators based on vertically aligned phage nanopillars. Energy Environ. Sci 2015, 8, 3198–3203.

(122). Lee J-H; et al. Vertical self-assembly of polarized phage nanostructure for energy harvesting. Nano Lett. 2019, 19, 2661–2667. [PubMed: 30875472]

(123). Wan Y; Xie L; Zhang X; Zhong Z Time dependence of piezoelectric d 33 coefficient of cellular ferroelectret polypropylene film. Appl. Phys. Lett 2011, 98, 122902.

(124). Park SM; et al. Fabrication of chiral M13 bacteriophage film by evaporation-induced self-assembly. Small 2021, 17, 2008097.

(125). Peivandi A; et al. Inducing Microscale Structural Order in Phage Nanofilament Hydrogels with Globular Proteins. ACS Biomaterials Science & Engineering 2022, 8, 340–347. [PubMed: 34905337]

(126). Tayeb P; Tayeb AH Nanocellulose applications in sustainable electrochemical and piezoelectric systems: A review. Carbohydr. Polym 2019, 224, 115149. [PubMed: 31472850]

(127). Sappati KK; Bhadra S Piezoelectric polymer and paper substrates: a review. Sensors 2018, 18, 3605. [PubMed: 30355961]

(128). Teodoro KB; et al. A review on the role and performance of cellulose nanomaterials in sensors. ACS sensors 2021, 6, 2473–2496. [PubMed: 34182751]

(129). Annamalai PK; Nanjundan AK; Dubal DP; Baek J-B An overview of cellulose-based nanogenerators. Advanced Materials Technologies 2021, 6, 2001164.

(130). Cao L; et al. Polysaccharides and proteins-based nanogenerator for energy harvesting and sensing: a review. Int. J. Biol. Macromol 2021, 173, 225–243. [PubMed: 33484800]

(131). Miao C; Reid L; Hamad WY Moisture-tunable, ionic strength-controlled piezoelectric effect in cellulose nanocrystal films. Applied Materials Today 2021, 24, 101082.

(132). Csoka L; et al. Piezoelectric effect of cellulose nanocrystals thin films. ACS Macro Lett. 2012, 1, 867–870. [PubMed: 35607134]

(133). Zhai L; Kim HC; Kim JW; Kim J Alignment effect on the piezoelectric properties of ultrathin cellulose nanofiber films. ACS Applied Bio Materials 2020, 3, 4329–4334.

(134). Wang J; et al. Piezoelectric nanocellulose thin film with large-scale vertical crystal alignment. ACS Appl. Mater. Interfaces 2020, 12, 26399–26404. [PubMed: 32427459]

(135). de Marzo G; et al. Sustainable, Flexible, and Biocompatible Enhanced Piezoelectric Chitosan Thin Film for Compliant Piezosensors for Human Health. Advanced Electronic Materials 2022, 2200069.

(136). Street RM; et al. Variable piezoelectricity of electrospun chitin. Carbohydr. Polym 2018, 195, 218–224. [PubMed: 29804971]

(137). Praveen E; Murugan S; Jayakumar K Investigations on the existence of piezoelectric property of a bio-polymer–chitosan and its application in vibration sensors. RSC Adv. 2017, 7, 35490–35495.

(138). Fukada E. Piezoelectricity of wood. J. Phys. Soc. Jpn 1955, 10, 149–154.

(139). Song Y; et al. Recent advances in cellulose-based piezo-electric and triboelectric nanogenerators for energy harvesting: a review. Journal of Materials Chemistry A 2021, 9, 1910–1937.

(140). Frka-Petesic B; Jean B; Heux L First experimental evidence of a giant permanent electric-dipole moment in cellulose nanocrystals. Europhys. Lett 2014, 107, 28006.

(141). Sriplai N; et al. Enhancing piezoelectric properties of bacterial cellulose films by incorporation of MnFe2O4 nanoparticles. Carbohydr. Polym. 2020, 231, 115730. [PubMed: 31888809]

(142). Wang L; et al. Flexible layered cotton cellulose-based nanofibrous membranes for piezoelectric energy harvesting and self-powered sensing. Carbohydr. Polym 2022, 275, 118740. [PubMed: 34742443]

(143). Zhang G; et al. Uniformly assembled vanadium doped ZnO microflowers/bacterial cellulose hybrid paper for flexible piezoelectric nanogenerators and self-powered sensors. Nano Energy 2018, 52, 501–509.

(144). Mahadeva SK; Walus K; Stoeber B Piezoelectric paper fabricated via nanostructured barium titanate functionalization of wood cellulose fibers. ACS Appl. Mater. Interfaces 2014, 6, 7547–7553. [PubMed: 24766163]

(145). Wu T; et al. High-performance nanogenerators based on flexible cellulose nanofibril/MoS2 nanosheet composite piezoelectric films for energy harvesting. Nano Energy 2021, 80, 105541.

(146). Choi HY; Jeong YG Microstructures and piezoelectric performance of eco-friendly composite films based on nanocellulose and barium titanate nanoparticle. Composites Part B: Engineering 2019, 168, 58–65.

(147). Wang R; et al. Engineered and Laser-Processed Chitosan Biopolymers for Sustainable and Biodegradable Triboelectric Power Generation. Adv. Mater 2018, 30, 1706267.

(148). Elieh-Ali-Komi D; Hamblin MR Chitin and chitosan: production and application of versatile biomedical nanomaterials. Int. J. Adv. Res 2016, 4, 411.

(149). Fukada E; Sasaki S Piezoelectricity of α-chitin. J. Polym. Sci., Polym. Phys. Ed 1975, 13, 1845–1847.

(150). Kalirajan C; Dukle A; Nathanael AJ; Oh T-H; Manivasagam G A Critical Review on Polymeric Biomaterials for Biomedical Applications. Polymers 2021, 13, 3015. [PubMed: 34503054]

(151). Wang X; Song J; Liu J; Wang ZL Direct-current nanogenerator driven by ultrasonic waves. Science 2007, 316, 102–105. [PubMed: 17412957]

(152). Cao X; et al. Piezoelectric Nanogenerators Derived Self-Powered Sensors for Multifunctional Applications and Artificial Intelligence. Adv. Funct. Mater 2021, 31, 2102983.

(153). Jenkins K; Kelly S; Nguyen V; Wu Y; Yang R Piezoelectric diphenylalanine peptide for greatly improved flexible nanogenerators. Nano Energy 2018, 51, 317–323.

(154). Vijayakanth T; Liptrot DJ; Gazit E; Boomishankar R; Bowen CR Recent Advances in Organic and Organic–Inorganic Hybrid Materials for Piezoelectric Mechanical Energy Harvesting. Adv. Funct. Mater 2022, 32, 2109492.

(155). Niu Z; et al. Recent advances in cellulose-based flexible triboelectric nanogenerators. Nano Energy 2021, 87, 106175.

(156). Maiti S; Karan SK; Kim JK; Khatua BB Nature driven bio-piezoelectric/triboelectric nanogenerator as next-generation green energy harvester for smart and pollution free society. Adv. Energy Mater 2019, 9, 1803027.

(157). Ghosh SK; Mandal D Efficient natural piezoelectric nanogenerator: electricity generation from fish swim bladder. Nano Energy 2016, 28, 356–365.

(158). Karan SK; et al. A new insight towards eggshell membrane as high energy conversion efficient bio-piezoelectric energy harvester. Materials today energy 2018, 9, 114–125.

(159). Maiti S; et al. Bio-waste onion skin as an innovative nature-driven piezoelectric material with high energy conversion efficiency. Nano Energy 2017, 42, 282–293.

(160). Yan Y; et al. Nanogenerators facilitated piezoelectric and flexoelectric characterizations for bioinspired energy harvesting materials. Nano Energy 2021, 81, 105607.

(161). Baláž M. Eggshell membrane biomaterial as a platform for applications in materials science. Acta biomaterialia 2014, 10, 3827–3843. [PubMed: 24681370]

(162). Hoque NA; et al. Biowaste crab shell-extracted chitin nanofiber-based superior piezoelectric nanogenerator. Journal of Materials Chemistry A 2018, 6, 13848–13858.

(163). Mariello M. Recent Advances on Hybrid Piezo-Triboelectric Bio-Nanogenerators: Materials, Architectures and Circuitry. Nanoenergy Advances 2022, 2, 64–109.

(164). Wang ZL Triboelectric nanogenerators as new energy technology and self-powered sensors–Principles, problems and perspectives. Faraday Discuss. 2014, 176, 447–458. [PubMed: 25406406]

(165). Ali F; Raza W; Li X; Gul H; Kim K-H Piezoelectric energy harvesters for biomedical applications. Nano Energy 2019, 57, 879–902.

(166). Zheng Q; Shi B; Li Z; Wang ZL Recent progress on piezoelectric and triboelectric energy harvesters in biomedical systems. Advanced Science 2017, 4, 1700029. [PubMed: 28725529]

(167). Ghosh SK; Mandal D Sustainable energy generation from piezoelectric biomaterial for noninvasive physiological signal monitoring. ACS Sustainable Chem. Eng 2017, 5, 8836–8843.

(168). Li H; et al. Carboxymethyl chitosan assembled piezoelectric biosensor for rapid and label-free quantification of immunoglobulin Y. Carbohydr. Polym 2022, 290, 119482. [PubMed: 35550770]

(169). Pohanka M. Overview of piezoelectric biosensors, immunosensors and DNA sensors and their applications. Materials 2018, 11, 448. [PubMed: 29562700]

(170). O'brien FJ Biomaterials & scaffolds for tissue engineering. Mater. Today 2011, 14, 88–95.

(171). Croisier F; Jérôme C Chitosan-based biomaterials for tissue engineering. European polymer journal 2013, 49, 780–792.

(172). Place ES; Evans ND; Stevens MM Complexity in biomaterials for tissue engineering. Nature materials 2009, 8, 457–470. [PubMed: 19458646]

(173). Rezvani Ghomi E; Nourbakhsh N; Akbari Kenari M; Zare M; Ramakrishna S Collagen-based biomaterials for biomedical applications. Journal of Biomedical Materials Research Part B: Applied Biomaterials 2021, 109, 1986–1999. [PubMed: 34028179]

(174). Ferreira AM; Gentile P; Chiono V; Ciardelli G Collagen for bone tissue regeneration. Acta biomaterialia 2012, 8, 3191–3200. [PubMed: 22705634]

(175). Chen C; Bai X; Ding Y; Lee I-S Electrical stimulation as a novel tool for regulating cell behavior in tissue engineering. Biomaterials research 2019, 23, 25. [PubMed: 31844552]

(176). Fernandez-Yague MA; et al. A Self-Powered Piezo-Bioelectric Device Regulates Tendon Repair-Associated Signaling Pathways through Modulation of Mechanosensitive Ion Channels. Adv. Mater 2021, 33, 2008788.

(177). Du L; et al. Design of high conductive and piezoelectric poly (3, 4-ethylenedioxythiophene)/chitosan nanofibers for enhancing cellular electrical stimulation. J. Colloid Interface Sci 2020, 559, 65–75. [PubMed: 31610306]

(178). Chen Y; et al. Piezoelectric and photothermal dual functional film for enhanced dermal wound regeneration via upregulation of Hsp90 and HIF-1α. Applied Materials Today 2020, 20, 100756.

(179). Prokhorov E; et al. Chitosan-BaTiO3 nanostructured piezopolymer for tissue engineering. Colloids Surf., B 2020, 196, 111296.

(180). Ribeiro C; Sencadas V; Correia DM; Lanceros-Méndez S Piezoelectric polymers as biomaterials for tissue engineering applications. Colloids Surf., B 2015, 136, 46–55.

(181). Goonoo N; Bhaw-Luximon A Piezoelectric polymeric scaffold materials as biomechanical cellular stimuli to enhance tissue regeneration. Materials Today Communications 2022, 31, 103491.

(182). Zaborowska M; et al. Microporous bacterial cellulose as a potential scaffold for bone regeneration. Acta biomaterialia 2010, 6, 2540–2547. [PubMed: 20060935]

(183). Leppik L; Oliveira KMC; Bhavsar MB; Barker JH Electrical stimulation in bone tissue engineering treatments. European Journal of Trauma and Emergency Surgery 2020, 46, 231–244. [PubMed: 32078704]

(184). Kuo CK; Marturano JE; Tuan RS Novel strategies in tendon and ligament tissue engineering: advanced biomaterials and regeneration motifs. BMC sports science, medicine and rehabilitation 2010, 2, 20.

(185). Elmessiery M. Physical basis for piezoelectricity of bone matrix. IEE Proc., Part A: Phys. Sci., Meas. Instrum., Manage. Educ 1981, 5, 336–346.

(186). šutka A; et al. Measuring piezoelectric output—fact or friction? Adv. Mater 2020, 32, 2002979.

(187). Ryu J; Lim SY; Park CB Photoluminescent peptide nanotubes. Adv. Mater 2009, 21, 1577–1581.

(188). Abbas M; Atiq A; Xing R; Yan X Silver-incorporating peptide and protein supramolecular nanomaterials for biomedical applications. J. Mater. Chem. B 2021, 9, 4444–4458. [PubMed: 33978051]

(189). Xie J; Liu W; Schultz PG A genetically encoded bidentate, metal-binding amino acid. Angew. Chem 2007, 119, 9399–9402.

(190). Gutierrez E; et al. 3D printing of antimicrobial alginate/bacterial-cellulose composite hydrogels by incorporating copper nanostructures. ACS Biomaterials Science & Engineering 2019, 5, 6290–6299. [PubMed: 33405536]

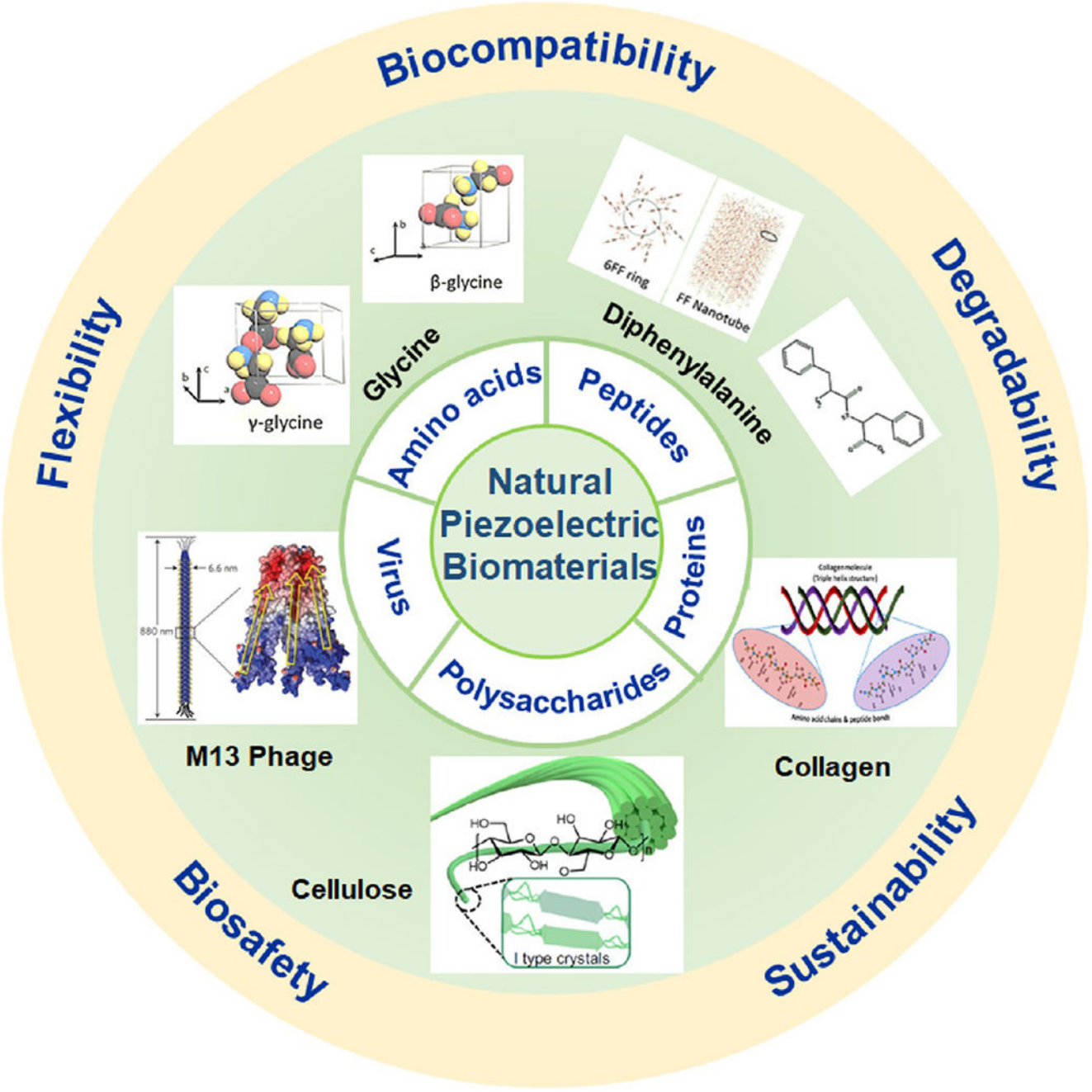

Figure 1.
Schematic of the five major types of natural piezoelectric biomaterials and their properties for biomedical applications.

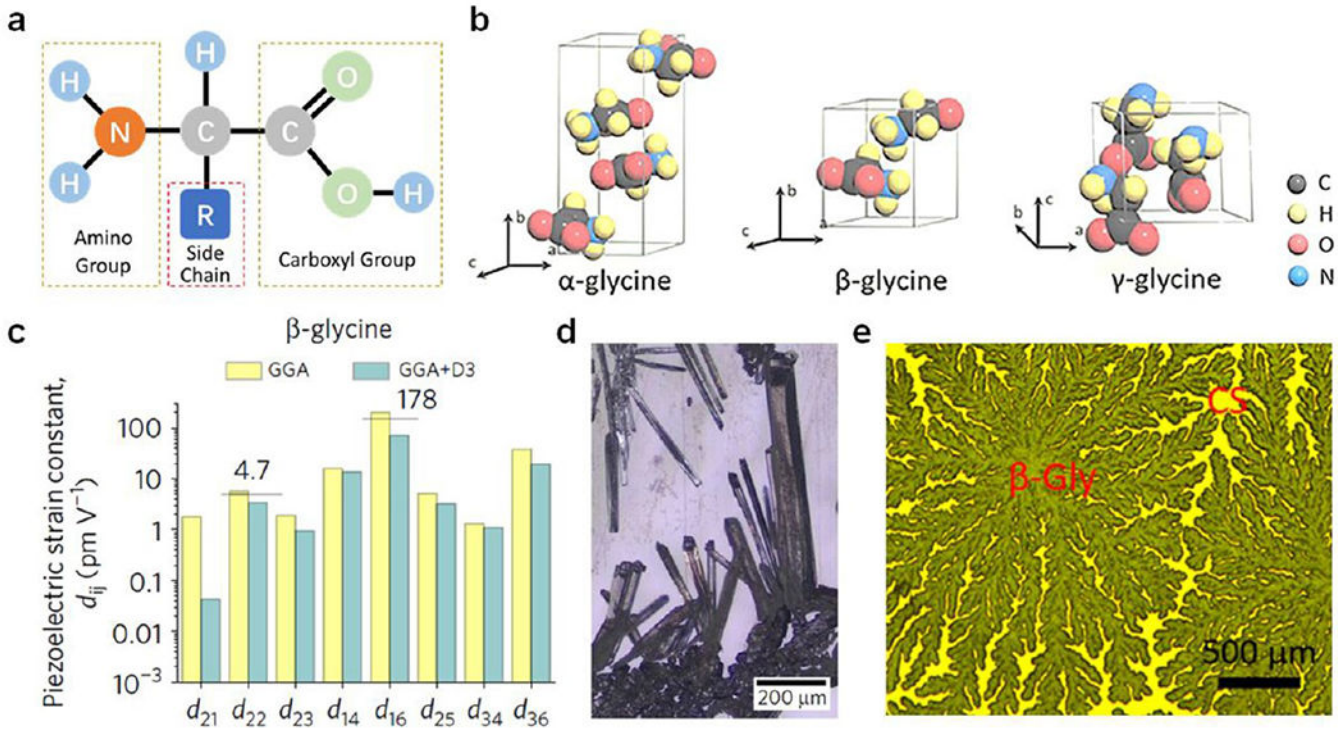

Figure 2.

Piezoelectric amino acids materials. (a) The general molecular structure of the amino acids. (b) Three atomic structures of glycine. Reprinted with permission under a Creative Commons CC BY License from ref 56. Copyright 2021 John Wiley and Sons. (c) Calculated piezoelectric coefficients for β-glycine. Experimental d_{22} and d_{16} values are marked above relevant columns. (d) Optical image of β-glycine needles. Reprinted with permission from ref 42. Copyright 2018 Springer Nature. (e) Optical microscopy image of chitosan (CS) film with β-glycine crystals (β-Gly). Reprinted with permission from ref 49. Copyright 2020 American Chemical Society.

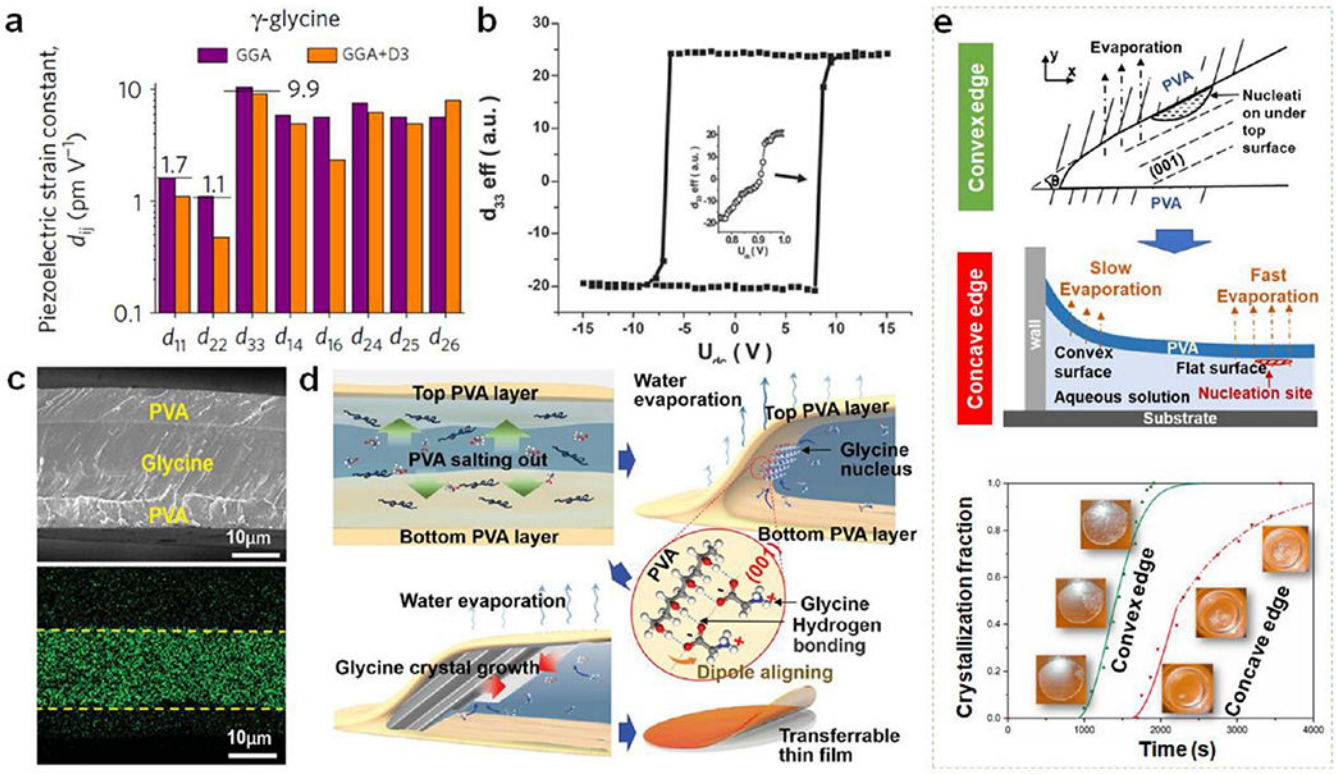

Figure 3.

Piezoelectric γ-glycine and scaling up. (a) Calculated piezoelectric coefficients for γ-glycine. Experimental d_{11}, d_{22}, and d_{33} values of d_{11}, d_{22}, and d_{33} values are marked. Reprinted with permission from ref 42. Copyright 2018 Springer Nature. (b) The piezoelectric hysteresis loop of γ-glycine microcrystal. Reprinted with permission from ref 62. Copyright 2012 John Wiley and Sons. (c) The cross-sectional SEM image of a PVA-glycine-PVA film and the corresponding EDS map of nitrogen (N). (d) Schematic illustration of PVA-glycine-PVA sandwich film formation Reprinted with permission from ref 37. Copyright 2021 American Association for the Advancement of Science. (e) Top: Schematics showing the nucleation site at the convex liquid edge moves to the center flat area when the liquid edge becomes concave. Bottom: Crystal growth kinetics of glycine-PVA films when the liquid film had a convex (green) or concave (red) edge. Reprinted with permission from ref 71. Copyright 2022 Royal Society of Chemistry.

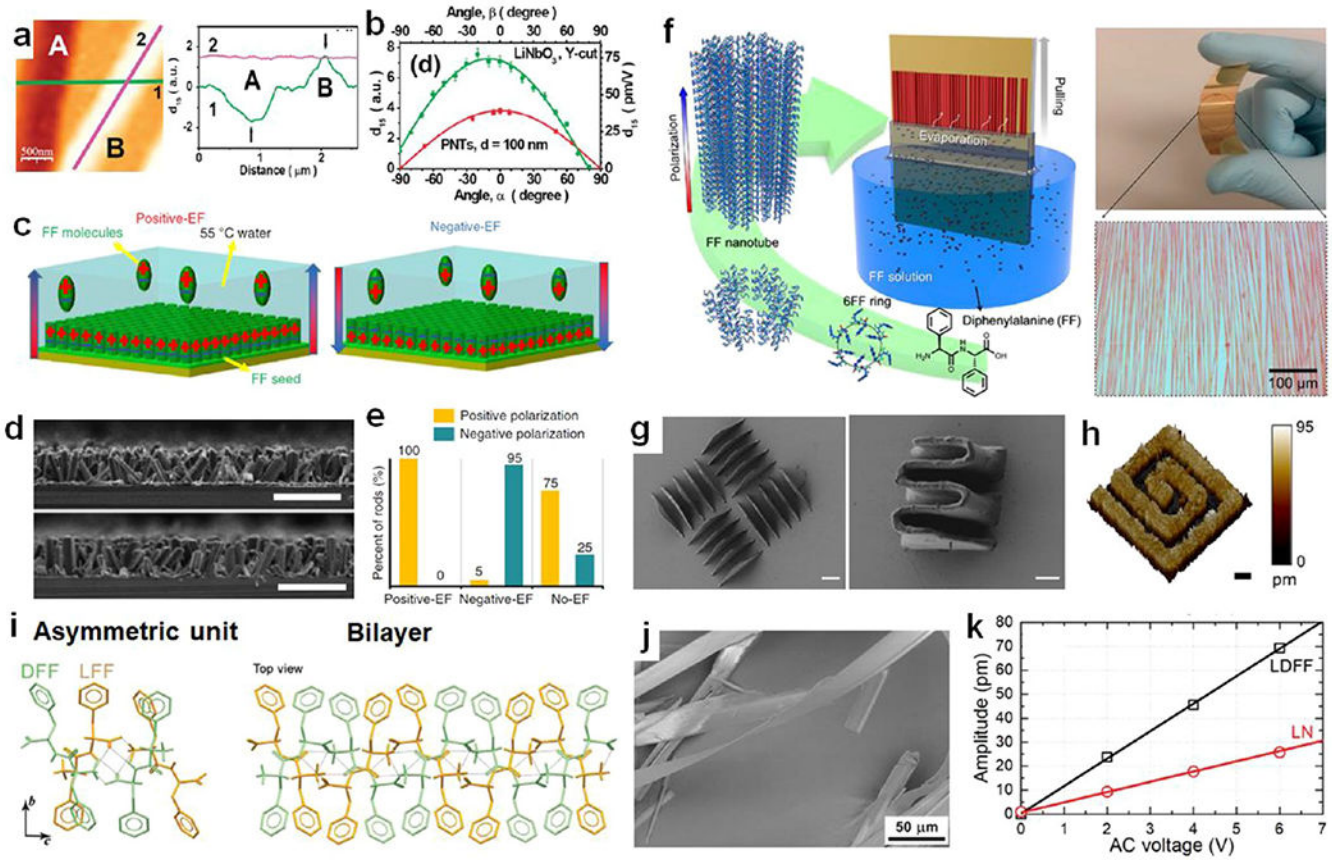

Figure 4.

Piezoelectric peptides. (a) PFM image and d_{33} distribution in two directions indicating opposite piezoelectric polarizations of two FF nanotubes. (b) In-plane piezoresponse angle dependence for PNTs and Y-cut $LiNbO_3$. Reprinted with permission from ref 65. Copyright 2010 American Chemical Society. (c) Illustration of FF microrods alignment under opposite electric field. (d) Cross-sectional SEM images of FF arrays under positive (up) and negative (bottom) electrical field (scale bars: 100 μm). (e) Statistics of polarization directions of FF microrods under positive, negative, and no electrical field. Reprinted with permission under a Creative Commons CC BY License from ref 43. Copyright 2016 Springer Nature. (f) Illustration of aligned FF nanotubes growth by Meniscus-driven dip-coating method. Digital photograph and optical microscopy image of FF nanotube array on a flexible substrate. Reprinted with permission from ref 78. Copyright 2018 American Chemical Society. (g) Field-emission scanning electron microscopy images of 3D-printed FF microstructures. An array of microwalls with an isosceles trapezoid shape (scale bar: 20 μm) and a zigzag wall (scale bar: 5 μm). (h) 3D PFM image of an after-annealed FF spiral pattern (scale bar: 3 μm). Reprinted with permission from ref 79. Copyright 2021 American Chemical Society. (i) The crystal structure of LDFF. (j) SEM image the LDFF tape. (k) Piezoresponse amplitude as a function of AC voltage of LDFF and lithium niobate (LN). Reprinted with permission from ref 80. Copyright 2021 John Wiley and Sons.

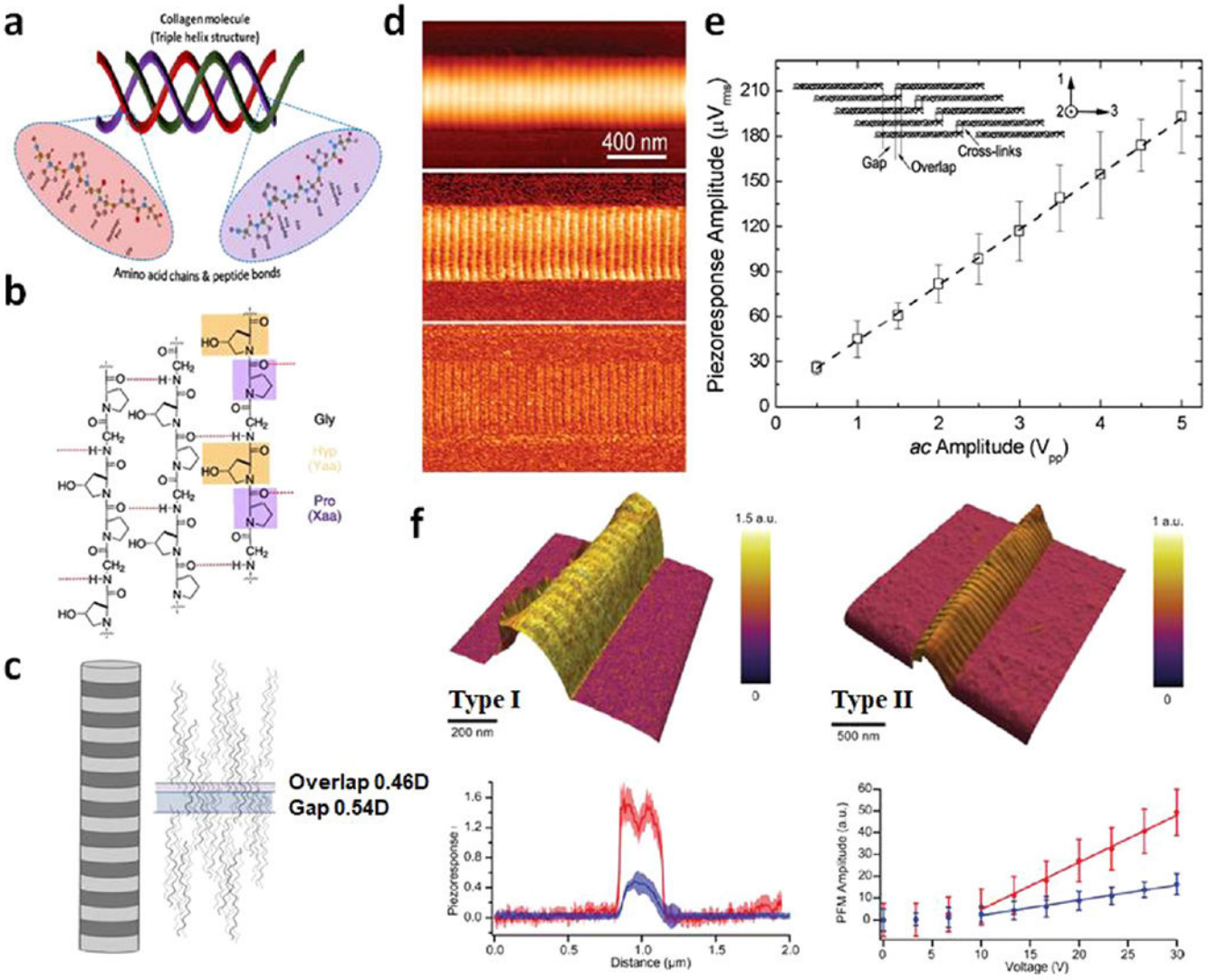

Figure 5.

Piezoelectric collagen structure and piezoresponses. (a) Illustration of collagen triple-helix structure formed by three twisted polypeptide chains. Reprinted with permission from ref 97. Copyright 2018 American Chemical Society. (b) The existence of interstrand hydrogen bonds. Reprinted with permission from ref 98. Copyright 2011 John Wiley and Sons. (c) Lateral structure of a collagen. Reprinted with permission from ref 99. Copyright 2022 John Wiley and Sons. (d) PFM topography image (top), piezoresponse amplitude image (mid) and the 2ω signal image (bottom) of a collagen fibril. (e) Shear piezoresponse as a function of applied voltage in the overlap region. Reprinted with permission from ref 100. Copyright 2009 American Chemical Society. (f) AFM images, corresponding averaged line profiles and amplitude dependence on AC voltage of type I (red) and type II (blue) collagen fibrils. Reprinted with permission from ref 101. Copyright 2014 AIP Publishing.

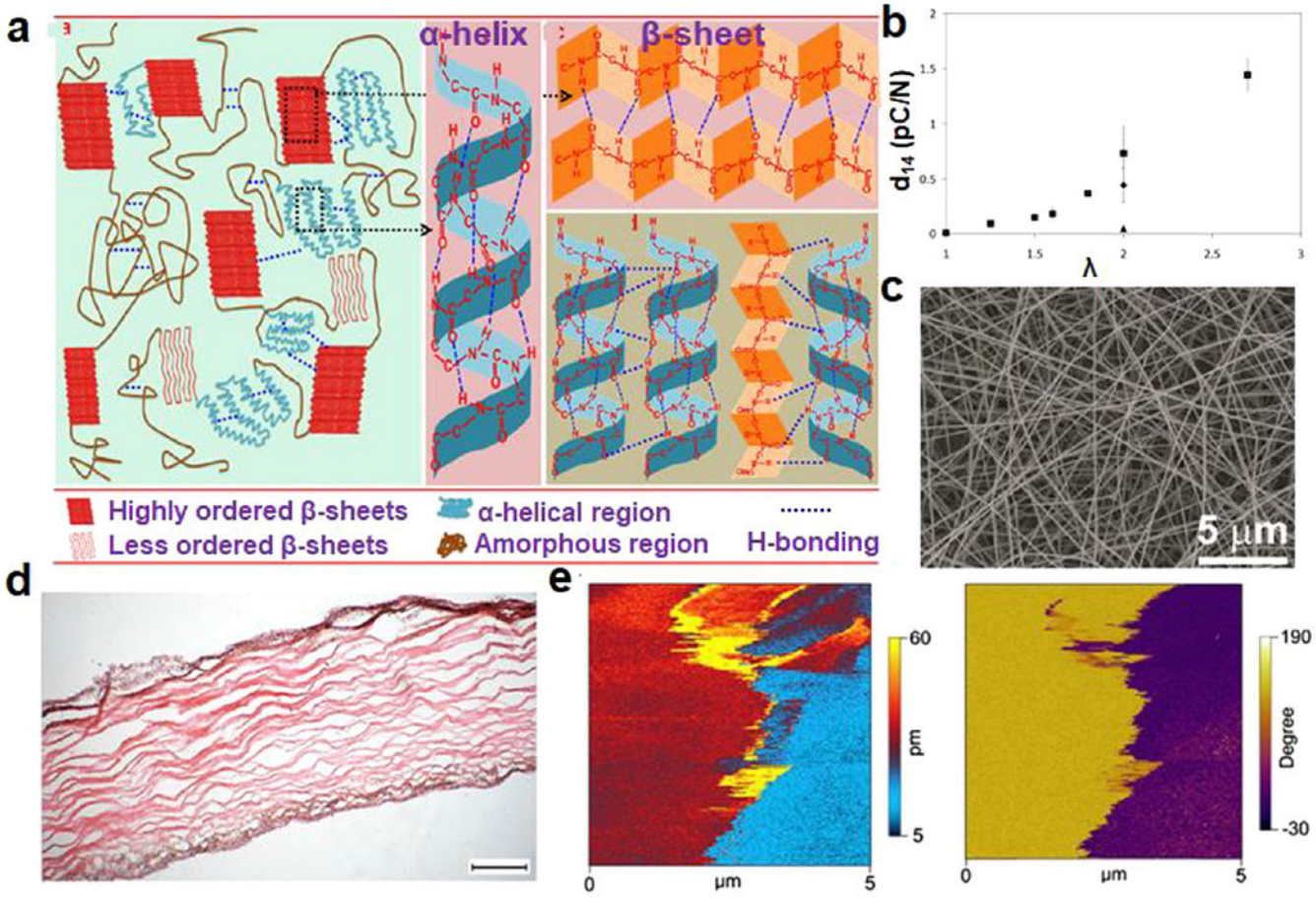

Figure 6.

Piezoelectric silk and elastin. (a) Schematic illustration of components and structures in spider silk. Reprinted with permission from ref 109. Copyright 2018 Elsevier. (b) The piezoelectric coefficient d_{14} of silk under different processing parameters (squares: zone drawn; triangles: water-immersion drawn; diamonds: methanol treated). Reprinted with permission from ref 45. Copyright 2011 John Wiley and Sons. (c) SEM image of electrospun silk fibroin. Reprinted with permission from ref 110. Copyright 2019 Elsevier. (d) Histological image of fibrous elastin (scale bar: 200 μm). (e) PFM mappings of elastin at high temperature (473 K). Reprinted with permission from ref 111. Copyright 2014 National Academy of Science.

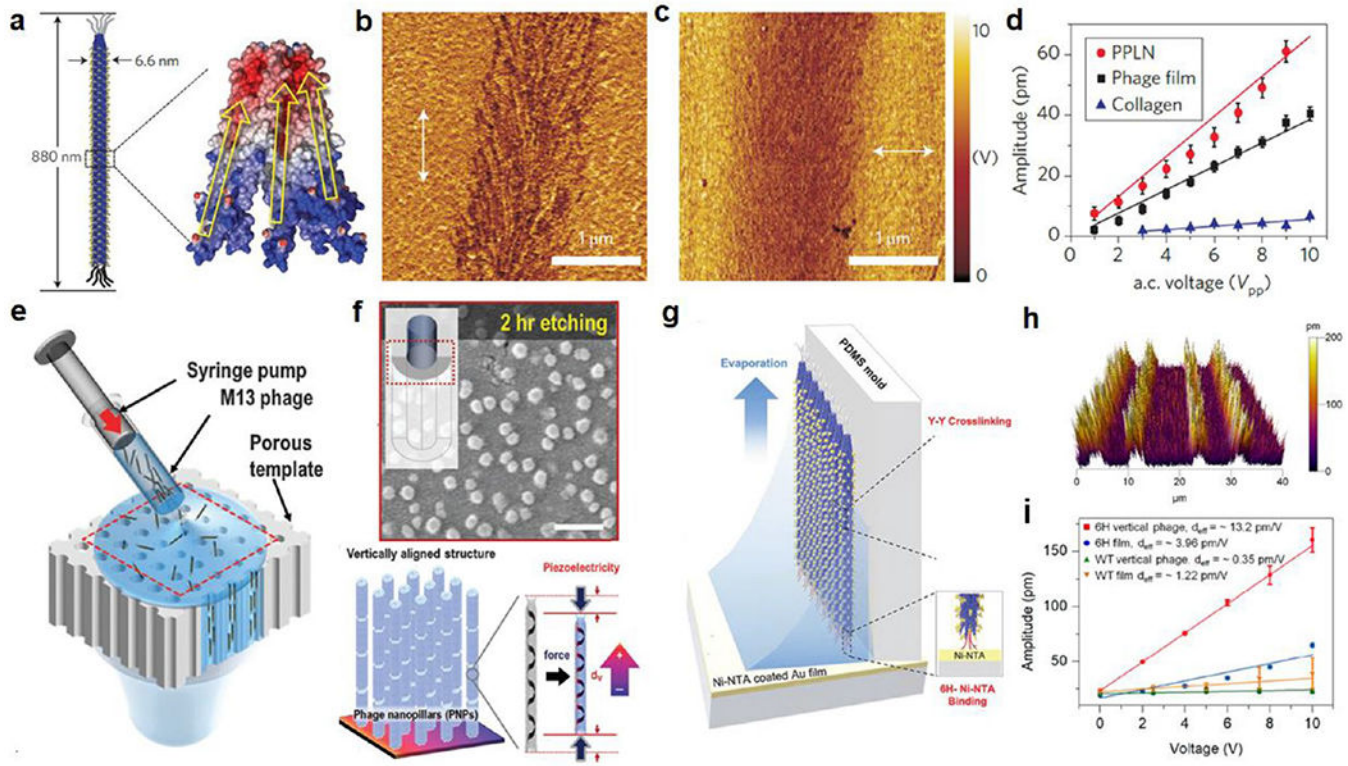

Figure 7.

Piezoelectric virus and assembling strategies. (a) Illustration of M13 phage structure with dipole directions indicated by yellow arrows. (b, c) PFM images of monolayer phage film scanning from two directions (indicated by white arrows). (d) Amplitude of piezoresponse–AC voltage curves from periodically poled lithium niobate (PPLN), phage film, and collagen. Reprinted with permission from ref 48. Copyright 2012 Springer Nature. (e) Illustration of the enforced infiltration strategy for fabrication of vertically aligned M13 phage nanopillars. (f) SEM image of the phage nanopillar-embedded porous template (scale bar = 200 nm) and schematic of phage nanopillars with axial aligned piezoelectricity. Reprinted with permission from ref 121. Copyright 2015 The Royal Society of Chemistry. (g) Schematic of the template-assisted method for growing vertically polarized phage nanostructure. (h) PFM amplitude image of vertically aligned phages. (i) The out-of-plane PFM amplitude dependence of applied voltage of genetically engineered (6H) and wildtype (WT) phage compared in film and vertical nanopillar forms. Reprinted with permission from ref 122. Copyright 2019 American Chemical Society.

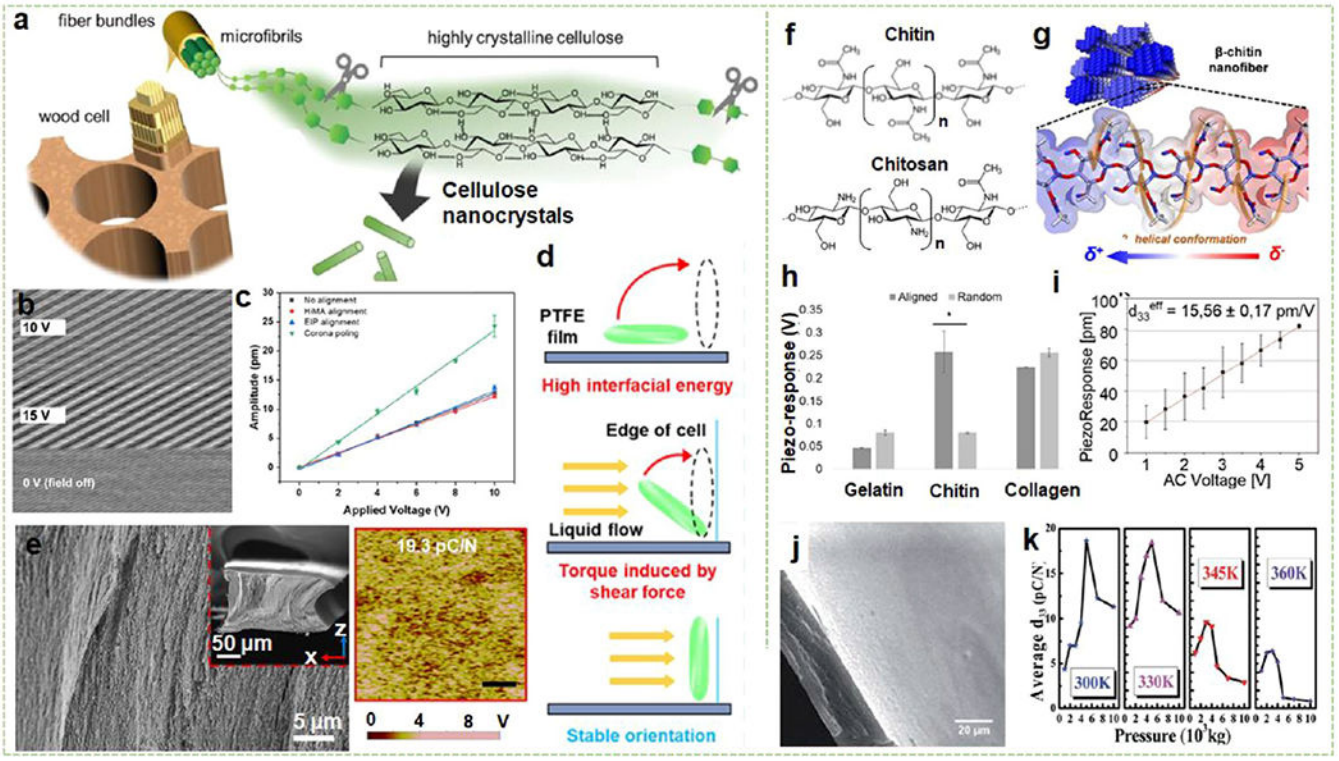

Figure 8.

Piezoelectric polysaccharides including cellulose and chitin/chitosan. (a) Schematic of CNC derived from wood pulp. Reprinted with permission from ref 131. Copyright 2021 Elsevier. (b) The AFM height deflection mapping of CNC film under different voltages. Reprinted with permission from ref 132. Copyright 2012 American Chemical Society. (c) Vertical displacement as a function of applied voltage for ultrathin CNF films under no alignment, HIMA and EIP alignment, and corona poling conditions. Reprinted with permission from ref 133. Copyright 2020 American Chemical Society. (d) Schematic of the vertical alignment mechanism. (e) Cross-sectional SEM image and surface PFM image of vertically aligned CNC film. Reprinted with permission from ref 134. Copyright 2020 American Chemical Society. (f) The molecular structures of chitin and chitosan. Reprinted with permission from ref 135. Copyright 2022 John Wiley and Sons. (g) Spontaneous polarization of β-chitin nanofibers. The arrow shows the polarization direction. Reprinted with permission from ref 40. Copyright 2018 Elsevier. (h) Piezoelectric response measured from gelatin, chitin, and collagen nanofibers nanogenerators. Reprinted with permission from ref 136. Copyright 2018 Elsevier. (i) Average piezoresponse dependence on AC voltage of chitosan film. Reprinted with permission from ref 135. Copyright 2022 John Wiley and Sons. (j) Cross-sectional SEM image of chitosan film prepared by using formic acid. (k) Average d_{33} values of chitosan films prepared by dissolving in formic acid dependence of pressure at different sintering temperatures. Reprinted with permission under a Creative Commons CC BY License from ref 137. Copyright 2017 The Royal Society of Chemistry.

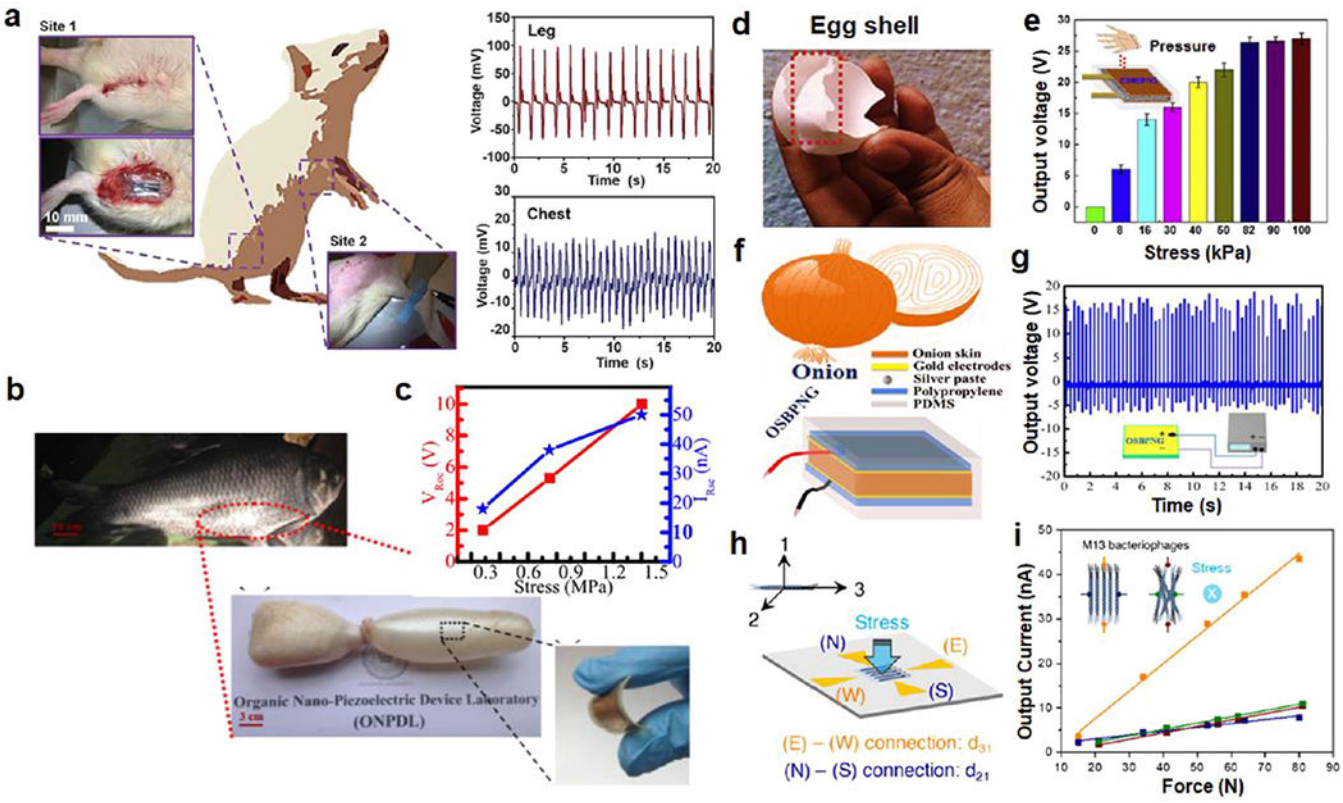

Figure 9.

Piezoelectric biomaterials for mechanical energy harvesting. (a) Schematic of a Sprague–Dawley rat and photographs of implanted glycine-PVA devices in rats. Corresponding voltage outputs of the glycine-PVA film driven at thigh and chest areas by different muscles. Reprinted with permission from ref 37. Copyright 2021 American Association for the Advancement of Science. (b) Photographs of the sweet water (*Catla Catla*) fish and its swim bladder. (c) The output voltages and currents dependence on stress generated by fish swim bladder NG. Reprinted with permission from ref 157. Copyright 2016 Elsevier. (d) Photograph of eggshell membrane. (e) The output voltages generated from eggshell membrane NG dependence on finger-tapped stress. Reprinted with permission from ref 158. Copyright 2018 Elsevier. (f) Illustration of the structure of piezoelectric NG made from onionskin (OSBPNG). (g) The generated output voltage from OSBPNG in forward connection. Reprinted with permission from ref 159. Copyright 2017 Elsevier. (h) Schematic illustration of electrode connections on quadrant electrode piezoelectric NG. (i) The output currents dependence on loading force for aligned phages and random phages. Reprinted with permission from ref 160. Copyright 2021 Elsevier.

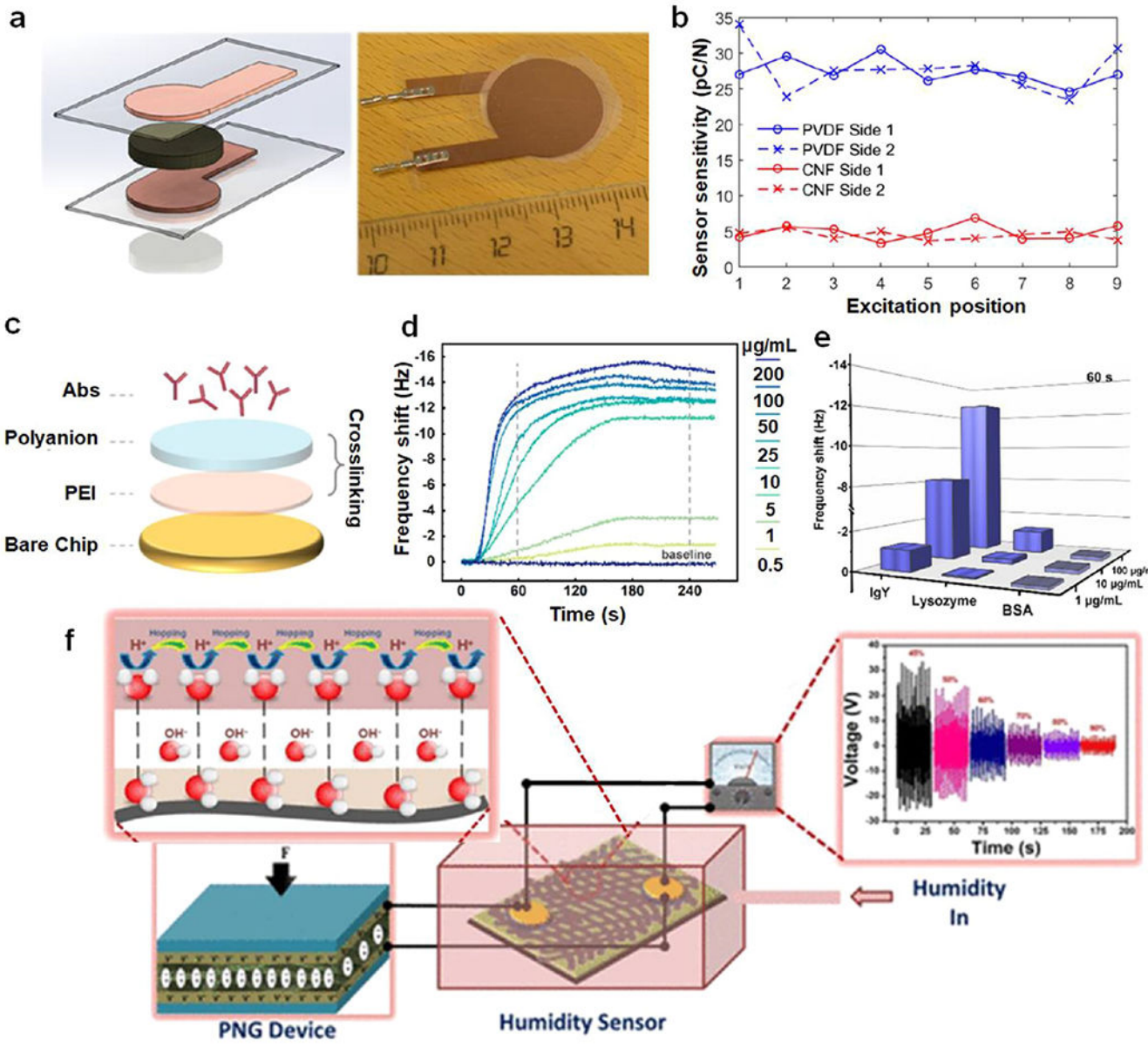

Figure 10.

Piezoelectric biomaterials for sensing. (a) Illustration of cellulose CNF sensor and the optical photograph of final device. (b) Piezoelectric sensitivity as a function of excitation position. Reprinted with permission from ref 47. Copyright 2016 American Chemical Society. (c) Schematic structure of carboxymethyl chitosan-based piezoelectric biosensor. (d) The response–time curves of a piezoelectric biosensor with different concentrations of additional IgY in PBS buffer. (e) The 3D sensor responses curve to IgY, lysozyme, and BSA with different concentrations at 60 s. Reprinted with permission from ref 168. Copyright 2022 Elsevier. (f) Schematic illustration of a self-powered collagen-based humidity sensor and output voltages under varied humidity. Reprinted with permission from ref 97. Copyright 2018 American Chemical Society.

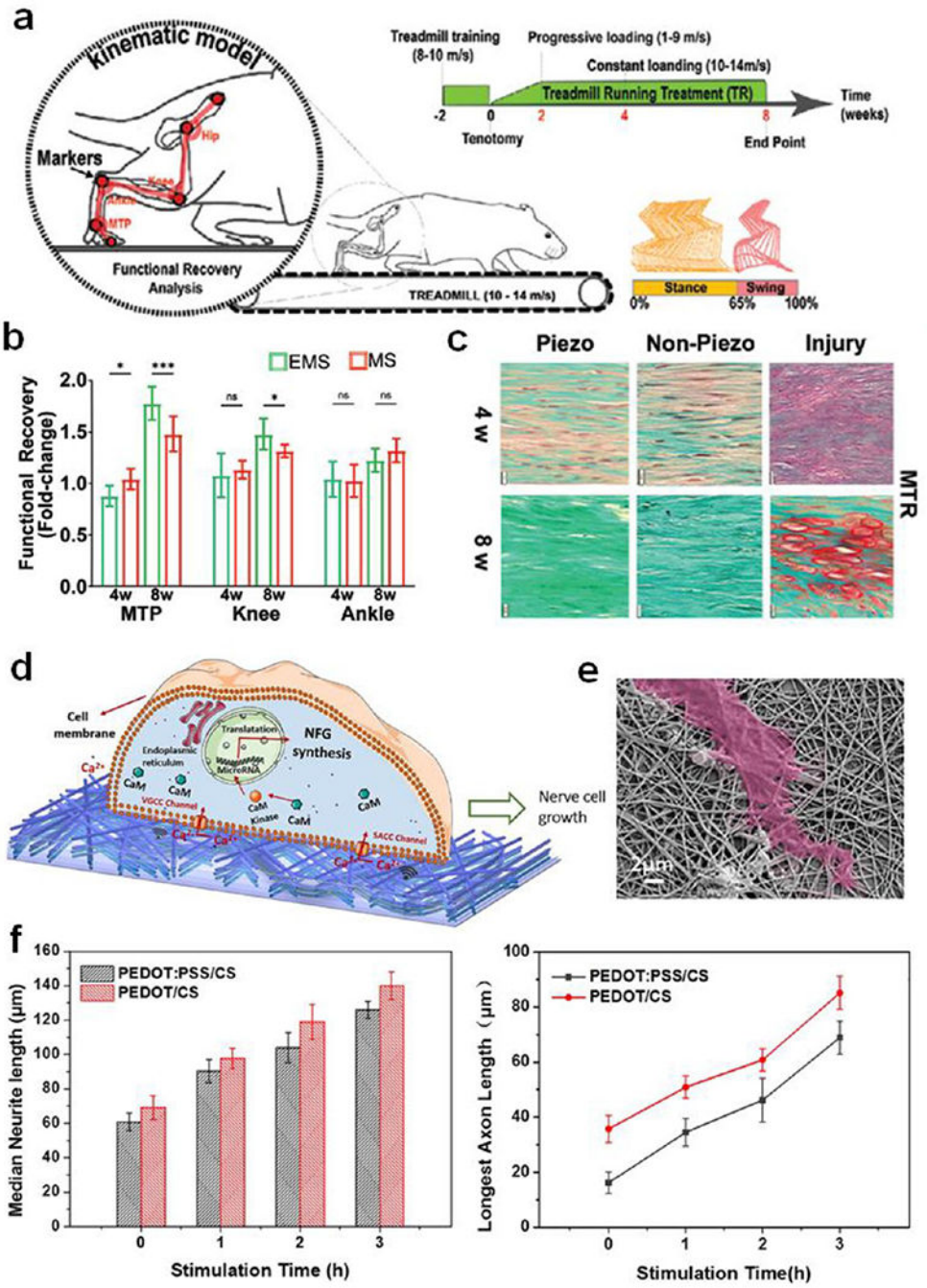

Figure 11.

Piezoelectric biomaterials for tissue engineering. (a) Schematic illustration of the kinematic model used to assess the functional recovery of tendon based on gait analyses and the MTR timeline. (b) The statistics of functional recovery in comparison under piezo (EMS) and nonpiezo (MS) conditions for metatarsophalangeal (MTP), knee, and ankle. (c) Histological images of MTR-treated EMS and MS groups after 4 and 8 weeks. Reprinted with permission under a Creative Commons CC BY License from ref 176. Copyright 2021 John Wiley and Sons. (d) A possible schematic of piezoelectically guided BNCs growth on PEDOT/chitosan

nanofibers substrate. (e) SEM image of BNCs cultured on PEDOT/chitosan nanofibers after 1 h of electrical stimulation. (f) Statistics of median neurite length of BNCs with different electrical stimulation time cultured on PEDOT:PSS/chitosan and PEDOT/chitosan substrates. Reprinted with permission from ref 177. Copyright 2020 Elsevier.

Table 1.

Comparison of the Piezoelectric Coefficients from Natural Piezoelectric Biomaterials

Type	Materials	Morphology	Piezoelectric coefficient	Ref
Amino Acids	*β*-glycine	Needle-shaped microcrystals	d_{16}: 178 pm V^{-1}	42
	β-glycine	Electrospun *β*-glycine/PVA nanofibers	d_{eff}: 12.5 pm V^{-1} d_{11}: 1.7 pm V^{-1}	70
	γ-glycine	Single crystals	d_{22}: −1.1 pm V^{-1} d_{33}: 9.93 pm V^{-1}	42
	γ-glycine	PVA-glycine-PVA sandwich heterostructure	d_{33}: 5.3 pC N^{-1}	37
	γ-glycine	PVA–glycine–PVA sandwich film	d_{33}: 6.13 pC/N	71
Peptides	Diphenylalanine (FF)	A 100 nm FF nanotube	d_{15}: 35 pm V^{-1}	65
	Diphenylalanine (FF)	Aligned vertical FF microrods arrays	d_{33}: 17.9 pm V^{-1}	43
	Diphenylalanine (FF)	Horizontally aligned FF nanotubes	d_{15}: 46.6 pm V^{-1}	78
	Fmoc-FF	Nanotubes	d_{15}: 33.7 pm V^{-1}	82
	cyclo-GW	Needlelike crystals	d_{14}: 4.6 pC N^{-1} d_{16}: 13.8 pC N^{-1}	83
	Boc-Dip-Dip	Tubular crystals	d_{33}: 73.1 pC N^{-1} d_{14}: – 12 pm V^{-1}	87
Proteins	Collagen	Rat tail tendon	d_{15}: 6.21 pm V^{-1} d_{33}: 0.89 pm V^{-1}	108
	Silk	Oriented silk II film	d_{14}: 1.5 pC N^{-1}	45
	Silk	Electrospun silk fibroin	d_{33}: 38 pm V^{-1}	110
	Elastin	Aortic elastin	d_{eff}: ~ 1 pm V^{-1}	117
Viruses	M13 phage	4E engineered M13 phage monolayer	d_{33}: 0.70 pm V^{-1}	48
	M13 phage	Vertically aligned 4E M13 phage nanopillars	d_{33}: 10.4 pm V^{-1}	121
	M13 phage	Vertically aligned M13 phage film	d_{eff}: 13.2 pm V^{-1}	122
Polysaccharides	Cellulose	Corona-poled ultrathin CNF film	d_{33}: 2.31 pm V^{-1}	133
	Cellulose	Vertically aligned CNC film	d_{33}: 19.3 pm V^{-1}	134
	Chitin	*β*-rich chitin film	d_{eff}: 3.986 pm V^{-1}	40
	Chitosan	Neutralized chitosan film	d_{33}: 15.56 pC N^{-1}	135